

# The role of snow cover affecting boreal-arctic soil freeze/thaw and carbon dynamics

Yonghong Yi<sup>1,\*</sup>, John S. Kimball<sup>1</sup>, Michael A. Rawlins<sup>2</sup>, Mahta Moghaddam<sup>3</sup>, Eugénie S. Euskirchen<sup>4</sup>

[1] Numerical Terradynamic Simulation Group (NTSG), College of Forestry and Conservation, The University of Montana, MT, USA, 59812

[2] Department of Geosciences, University of Massachusetts, Amherst MA, USA

[3] Department of Electrical Engineering, University of Southern California, CA, USA

[4] Institute of Arctic Biology, University of Alaska Fairbanks, Fairbanks AK, USA

Correspondence to: Yonghong Yi (yonghong.yi@ntsg.umt.edu)

## Abstract

Northern Hemisphere permafrost affected land areas contain about twice as much carbon as the global atmosphere. This vast carbon pool is vulnerable to accelerated losses through mobilization and decomposition under projected global warming. Satellite data records spanning the past 3 decades indicate widespread reductions ( $\sim 0.8\text{-}1.3$  days decade<sup>-1</sup>) in the mean annual snow cover extent and frozen season duration across the pan-Arctic domain, coincident with regional climate warming trends. How the soil carbon pool responds to these changes will have a large impact on regional and global climate. Here, we developed a coupled terrestrial carbon and hydrology model framework with detailed 1-D soil heat transfer representation to investigate the sensitivity of soil organic carbon stocks and soil decomposition to climate warming and changes in snow cover conditions in the Pan-Arctic region over the past three decades (1982-2010). Our results indicate widespread soil active layer deepening across the pan-Arctic, with a mean decadal trend of  $6.6 \pm 12.0$  (SD) cm, corresponding with widespread warming. Warming promotes vegetation growth and soil heterotrophic respiration particularly within surface soil layers ( $\leq 0.2$  m). The model simulations also show that seasonal snow cover has a large impact on soil temperatures,

1 whereby increases in snow cover promote deeper ( $\geq 0.5$  m) soil layer warming and soil  
2 respiration, while inhibiting soil decomposition from surface ( $\leq 0.2$  m) soil layers, especially in  
3 colder climate zones (mean annual  $T \leq -10$  °C). Our results demonstrate the important control of  
4 snow cover in affecting northern soil freeze/thaw and soil carbon decomposition processes, and  
5 the necessity of considering both warming, and changing precipitation and snow cover regimes  
6 in characterizing permafrost soil carbon dynamics.

7

## 8 **1 Introduction**

9 The northern high latitudes contain about twice as much carbon as the global atmosphere, largely  
10 stored in permafrost and seasonally thawed soil active layers (Hugelius et al., 2014). This vast  
11 carbon pool is vulnerable to accelerated losses through mobilization and decomposition under  
12 regional warming, with potentially large global carbon and climate impacts (Koven et al., 2011;  
13 Schaefer et al., 2011; Schuur et al., 2015). The northern high latitudes have experienced a much  
14 stronger warming rate than the global average over recent decades (Serreze and Francis, 2006),  
15 and this warming trend is projected to continue, along with a general increase in surface  
16 precipitation (Solomon et al., 2007). A better understanding of how the northern soil carbon pool  
17 responds to these changes is critical to predict climate feedbacks and associated impacts to  
18 northern ecosystems.

19 Potential vulnerability of soil carbon to mobilization and accelerated decomposition with climate  
20 warming, particularly in permafrost areas, will largely depend on changes in soil moisture and  
21 thermal conditions (Grosse et al., 2011; Schaefer et al., 2011; Schuur et al., 2015). Widespread  
22 soil thawing and permafrost degradation in the boreal and Arctic have been reported (e.g.  
23 Jorgenson et al., 2006; Romanovsky et al., 2010a, b). This has triggered a series of changes in  
24 boreal and Arctic ecosystems, including changes in lake and wetland areas (Smith et al., 2005;  
25 Watts et al., 2012), tundra shrub cover expansion (Tape et al., 2006; Sturm et al., 2005),  
26 thermokarst and other disturbances (Grosse et al., 2011), which are likely having a profound  
27 influence on both surface and subsurface hydrology, and biogeochemical cycles. In particular,  
28 increases in soil temperature and associated soil thawing potentially expose vast soil organic  
29 carbon stocks, formally stabilized in perennial frozen soils, to mobilization and decomposition,  
30 which may promote large positive climate feedbacks (Schaefer et al., 2011; Schuur et al., 2015).

1 Previous studies have highlighted the importance of both surface air temperature and snow cover  
2 conditions affecting the soil thermal regime among many other factors (Stieglitz et al., 2003;  
3 Zhang, 2005; Osterkamp, 2007; Lawrence and Slater, 2010; Romanovsky et al., 2010a). Changes  
4 in the rate of accumulation, timing, duration, density and amount of snow cover during the  
5 winter season play an important role in determining how soil responds to surface warming due to  
6 strong insulation effects of snow cover on ground temperature and its role in the surface energy  
7 budget (Zhang, 2005). Both surface warming and a changing precipitation regime can modify  
8 seasonal snow cover conditions, leading to a non-linear soil response to warming (Lawrence and  
9 Slater, 2010). Increases in winter precipitation and deepening of the snowpack may enhance soil  
10 warming, while a reduced snowpack, due to precipitation decreases or warming-enhanced snow  
11 sublimation, may promote soil cooling. Changes in snow cover duration and condition can also  
12 alter the amount of energy absorbed by the ground and modify the rate of soil warming  
13 (Euskirchen et al., 2007). The Arctic is expected to experience continued warming and  
14 precipitation increases under projected climate trends (Solomon et al., 2007); how these climate  
15 trends will affect soil moisture and thermal dynamics is a key question affecting potential  
16 changes in northern soil carbon dynamics and associated climate feedbacks.

17 Satellite data records over the past three decades (1979-2011) indicate widespread reductions  
18 ( $\sim 0.8\text{-}1.3$  days decade<sup>-1</sup>) in mean annual snow cover extent and frozen season duration across the  
19 pan-Arctic domain, coincident with regional warming (Brown and Robinson, 2011; Kim et al.,  
20 2012). Earlier onset of spring snow melt and soil thaw has been observed from both in situ  
21 ground and satellite measurements, while the onset of snow cover and soil freezing in the fall  
22 show more variable trends (Brown and Robinson, 2011; Kim et al., 2012). More active snow  
23 melt during the snow season, largely in the early snow season, has also been observed from  
24 satellite observations of regional snow cover extent and surface freeze/thaw cycles (Kim et al.,  
25 2015). On the other hand, snow depth trends in the boreal/Arctic region show large spatial  
26 variability. For example, several studies have shown a general snow depth increase in eastern  
27 Siberia (e.g. Park et al., 2014) and decrease in western North America in recent decades (Dyer  
28 and Mote, 2006).

29 The objective of this study is to assess how northern soil thermal and carbon dynamics respond  
30 to surface warming and changes in snow cover conditions during the satellite era (since 1979).  
31 To that end, we developed a coupled hydrology and carbon model framework with detailed soil

1 heat transfer representation adapted for the pan-Arctic basin and Alaska domain. We used this  
2 model to investigate recent climate-related impacts on soil thermal and carbon dynamics over the  
3 past three decades (1982-2010). We conducted a sensitivity analysis by running the model with  
4 different configurations of surface meteorology inputs to evaluate how soil thermal conditions  
5 and soil carbon dynamics respond to changes in air temperature and precipitation during the  
6 same period.

7

## 8 **2 Methods**

### 9 **2.1 Model description**

10 A coupled hydrology and carbon model was used to investigate sensitivity of the soil thermal  
11 regime and soil carbon decomposition to changes in surface air temperature and snow cover  
12 conditions. The hydrology model accounts for the effects of soil organic layers, changes in  
13 surface snow cover properties and soil water phase change on the soil freeze/thaw process in  
14 permafrost landscapes (Rawlins et al., 2013). These factors represent important controls on soil  
15 thermal dynamics within the active layer (Nicolsky et al., 2007; Lawrence and Slater, 2008;  
16 Lawrence and Slater, 2010), enabling improved estimation of subsurface soil temperature and  
17 moisture profiles, particularly in permafrost areas, and representation of essential environmental  
18 constraints on soil carbon decomposition.

19 The hydrology model used for this investigation is an extension of previous efforts on large-scale  
20 pan-Arctic water balance modeling (PWBM, Rawlins et al., 2003; Rawlins et al., 2013). Recent  
21 updates to the model include improved simulation of snow/ground and subsurface temperature  
22 dynamics using a 1-D heat transfer equation (Rawlins et al., 2013), instead of the empirical thaw  
23 depth estimation based on the Stefan solutions used in Rawlins et al. (2003). The updated  
24 PWBM model has 23 soil layers down to 60 m below surface, with increasing layer thickness at  
25 depth. Up to five snow layers are used to account for the effects of seasonal snow cover  
26 evolution on the ground thermal regime, and changes in seasonal snow density and thermal  
27 conductivities are also considered. Other model improvements include accounting for the impact  
28 of soil organic carbon content on soil thermal and hydraulic properties (Appendix A1, Eq. A3),

1 which is an important feature of boreal and Arctic soils (Lawrence and Slater, 2008). Further  
2 details on the updated hydrology model are provided in Appendix A1.

3 A satellite-based terrestrial carbon flux (TCF) model (Yi et al., 2013) was coupled to the  
4 hydrology model for this investigation. The TCF model uses a light use efficiency algorithm  
5 driven by satellite estimates of FPAR (Fraction of vegetation canopy intercepted  
6 Photosynthetically Active Radiation) to estimate vegetation productivity and litterfall inputs to a  
7 soil decomposition model. In the original TCF model, soil carbon stocks and respiration fluxes  
8 were estimated using a simplified three-pool soil organic carbon (SOC) decomposition  
9 framework with environmental constraints on soil decomposition rates derived from either  
10 satellite-estimated surface soil moisture and temperature fields (Kimball et al., 2009) or  
11 reanalysis data (Yi et al., 2013). This approach assumes that the major source of soil  
12 heterotrophic respiration (Rh) comes from surface ( $\leq 10$  cm) litter and surface organic layers.  
13 However, the contribution of deeper soils to total Rh may be non-negligible, especially in high  
14 latitude boreal and Arctic tundra landscapes with characteristic carbon-rich soils (Koven et al.,  
15 2011; Schuur et al., 2015). Therefore, in this study, we incorporated a more detailed soil  
16 decomposition model representing SOC stocks extending to 3 m below the surface, and  
17 representing differences in litterfall and soil organic matter substrate quality within the soil  
18 profile (Thornton et al., 2002). The resulting soil decomposition model used for this study  
19 includes three litterfall pools, three SOC pools with relatively fast turnover rates and a deep SOC  
20 pool with a slow turnover rate (Fig. S1). The three litterfall pools were distributed within the top  
21 20 cm of the soil layers; the three fast SOC pools were distributed within the top 50 cm of the  
22 soil layers, and the deep SOC pool extended from 50 cm to 3 m below the surface. Substantial  
23 SOC may be stored in permafrost soils below 3 m depth (Hugelius et al., 2014), and may  
24 potentially undergo mobilization with continued warming. However, this contribution to total  
25 land-atmosphere carbon (CO<sub>2</sub>) exchange was assumed negligible for the recent historical period  
26 examined (Schaefer et al., 2011) and was not considered in this study. Further details on the  
27 carbon model used in this study are provided in Appendix A2.

## 28 **2.2 Datasets**

29 The modeling domain for this investigation encompasses the pan-Arctic drainage basin and  
30 Alaska, representing a total land area extent of approximately 24.95 million km<sup>2</sup>. The model was

1 run at a 25-km northern hemisphere Equal-Area Scalable Earth Grid (EASE-Grid) spatial  
2 resolution and daily time step from 1979 to 2010. Further details on the model validation datasets  
3 and inputs used for this study are provided below.

#### 4 **2.2.1 In situ data**

5 In situ measurements from 20 Eddy Covariance (EC) tower sites across the pan-Arctic domain  
6 were obtained from the La Thuile FLUXNET dataset (Baldocchi, 2008), and were used to  
7 evaluate the model simulated daily carbon fluxes, and soil temperature and moisture fields  
8 (Table S1). These tower sites represent major vegetation community types across the study  
9 domain and have at least one year of observations available. For validation, the model was  
10 driven using tower observed meteorology. The tower daily carbon flux observations are derived  
11 from half-hourly EC CO<sub>2</sub> flux measurements that have been processed and aggregated using  
12 consistent gap filling and quality control procedures (Baldocchi, 2008). Limited surface ( $\leq 15$  cm)  
13 soil temperature and moisture measurements were also provided at a portion of the tower sites,  
14 but with unknown soil sampling depths and very few measurements at the tundra sites. Therefore,  
15 we selected one boreal forest and one tundra site with detailed in situ measurements (including  
16 carbon fluxes, soil temperature and soil moisture) for additional model evaluation (Table 1). The  
17 boreal forest site represents a single tower, whereas the tundra site includes three towers  
18 representing three different tundra community types.

19 The tundra site is located within the Imnavait Creek watershed in the northern foothills of the  
20 Brooks Range, Alaska (68°37'N, 149°18'W), and underlain with continuous permafrost  
21 (Euskirchen et al., 2012). Mean annual air temperature and precipitation at the site is -7.4 °C and  
22 318 mm with about 40% and 60% of annual precipitation occurring as rain and snow,  
23 respectively. There are three towers in three different tundra community types, including dry  
24 heath, moist acidic tussock and wet sedge tundra. The surface soil organic layer thickness varies  
25 from 34.0±2.4 cm in wet sedge tundra to 2.3±0.3 cm for dry heath tundra. The maximum active  
26 layer thaw depth varies from ~40 cm at the dry heath site to ~70 cm at the tussock tundra site  
27 (Euskirchen et al., 2012). Soil temperature and moisture at 5 cm depth were measured within  
28 each tundra tower footprint. All observations including carbon fluxes and soil temperature and  
29 moisture are available from 2008 to 2011.

1 The boreal forest site used in this study is part of a network of tower EC sites spanning a fire  
2 chronosequence in central Manitoba (55°54'N, 98°31'W) at various stages of succession  
3 following large stand replacement fires (Goulden et al., 2011). We chose one of the two oldest  
4 chronosequence tower sites burned in year 1930 for model validation because this site had more  
5 continuous measurements of carbon fluxes and surface meteorology, and high quality data  
6 (indicated by the tower metadata) during the observation period (2002-2005). This site is  
7 dominated by mature closed-canopy black spruce stands. The mean annual air temperature and  
8 precipitation at this site are -3.2°C and 520 mm respectively. Soil temperatures were measured at  
9 the surface (0 cm) and at multiple (6, 11, 16, 18, 29, 41 and 55 cm) soil depths, while soil  
10 moisture was also measured at multiple (11, 18, 28, 41 and 55 cm) depths.

### 11 **2.2.2 Model inputs**

12 Primary model drivers include daily surface meteorology and satellite-based normalized  
13 difference vegetation index (NDVI) records. Daily average and minimum air temperature,  
14 precipitation, wind speed, atmosphere vapor pressure deficit (VPD) and downward solar  
15 radiation were obtained from a new version of the WATCH Forcing Data (WFD) applied to  
16 ERA-Interim reanalysis (WFDEI; Weedon et al., 2014). This dataset was created by extracting  
17 and interpolating the ERA-Interim reanalysis to 0.5°×0.5° spatial resolution with sequential  
18 elevation correction of surface meteorological variables and monthly bias correction from  
19 gridded observations including CRU TS (v3.1 and v3.2) and GPCC (v5 and v6) datasets (for  
20 precipitation only). The daily WFDEI surface meteorology data is available from 1979 to 2010  
21 and allows more thorough comparisons of hydrological model outputs with other relevant  
22 satellite products than the previous WFD dataset (Weedon et al., 2014). The third-generation  
23 Global Inventory Monitoring and Modelling Studies (GIMMS3g) NDVI dataset (Xu et al., 2013)  
24 was used to estimate litterfall seasonality and FPAR, as critical inputs to the TCF model (Yi et  
25 al., 2013). The GIMMS3g dataset was assembled from different NOAA Advanced Very High  
26 Resolution Radiometer (AVHRR) sensor records, accounting for various deleterious effects  
27 including calibration loss, orbital drift and volcanic eruptions. The NDVI data has a 15-day  
28 temporal repeat and 8km spatial resolution, extending from 1982 to 2010. For the model  
29 simulations, both WFDEI and GIMMS3g forcing datasets were re-gridded to a consistent 25 km  
30 EASE-GRID format and the bimonthly GIMMS3g data was interpolated to a daily time step.

1 The NDVI data from year 1982 were used as drivers for model spin-up and simulations prior to  
2 the start of the GIMMS3g observation record (i.e. 1979-1981).

3 Other ancillary model inputs included a merged 8-km land cover dataset (Bi et al., 2013)  
4 combining the 500 m MODIS International Geosphere-Biosphere Programme (IGBP) land cover  
5 map (Friedl et al., 2010) and the Circumpolar Arctic Vegetation Map (CAVM; Walker et al.,  
6 2005). The CAVM was used to identify tundra vegetation within the circumpolar region as a  
7 supplement to the IGBP classification, which does not provide a specific category for tundra and  
8 forest-tundra transition biome types (Bi et al., 2013). The dominant land cover type within each  
9 25 km EASE Grid cell was chosen based on the merged 8-km land cover dataset and reclassified  
10 according to the original PWBM land cover classification (Rawlins et al., 2013; Fig. S2). Tundra,  
11 forest-tundra and taiga/boreal biomes account for approximately 70% of the total pan-Arctic  
12 drainage basin area (Fig. S2).

13 Soil organic carbon inventory data (GSDT, 2000; Hugelius et al., 2014) were used to prescribe  
14 the SOC fraction in each model soil layer. The fraction of SOC has a large impact on soil  
15 thermal and hydraulic properties, and is therefore an important control on characterizing soil  
16 freeze/thaw and moisture processes (Lawrence and Slater, 2008; Nicolsky et al., 2007). The  
17 IGBP Global Soil Data Task (GSDT, 2000) and the Northern Circumpolar Soil organic Carbon  
18 Database (NCSCD; Hugelius et al., 2014) SOC data was distributed through the top 11 model  
19 soil layers ( $\leq 1.4$  m depth) across the study area following Rawlins et al. (2013) and Lawrence  
20 and Slater (2008). The NCSCD data, which provides an updated estimate of SOC in permafrost  
21 affected areas, was used to prescribe the SOC fraction for permafrost areas, while the GSDT data  
22 was applied to non-permafrost areas. Generally, the organic carbon fraction within the top 5 soil  
23 layers ( $\leq 23$  cm depth) is high, with mean values of 53.7% and 39.4% for the two deeper surface  
24 soil layers (13-23 cm depth) averaged over the pan-Arctic domain.

### 25 **2.3 Model parameterization**

26 A dynamic litterfall allocation scheme based on satellite NDVI data (Appendix A2) was used to  
27 prescribe the daily litterfall fraction through each annual cycle to account for litterfall seasonality,  
28 particularly for deciduous vegetation types (Randerson et al., 1996; White et al., 2000). The  
29 GIMMS3g NDVI bimonthly data was first aggregated to a monthly time step and then used to



1 characterize monthly leaf loss and turnover rates of fine roots during the active growth period  
2 based on Eq. (A7). The monthly litterfall fraction was then evenly distributed on a daily time  
3 step within each month. This approach generally allocates more litterfall during the latter half of  
4 the growing season, while the model simulations show generally more soil heterotrophic  
5 respiration during the latter portion of the year (Fig. S3). A comparison of model simulations  
6 against tower measurements shows overall improved NEE seasonality relative to a previous TCF  
7 model application where litterfall was distributed evenly over the annual cycle (Yi et al. 2013).

## 8 **2.4 Model sensitivity analysis**

9 We conducted a model sensitivity analysis to examine how the estimated soil thermal regime and  
10 SOC decomposition respond to changes in surface air temperature and snow conditions over the  
11 most recent three decades. Three sets of daily model simulations were run by: 1) varying air  
12 temperature (T) and precipitation (P) inputs; 2) varying T inputs alone (temperature sensitivity  
13 analysis), and 3) varying P inputs alone (precipitation sensitivity analysis). Daily mean T  
14 (including daily mean and minimum temperature) and P climatology was first derived from the  
15 initial three-year (1979-1981) WFDEI meteorological record and used in the model sensitivity  
16 runs. The daily climatology, based on three-year (1979-1981) meteorological records rather than  
17 a single year (i.e. 1979), was used to minimize effects from characteristically large climate  
18 fluctuations in the northern high latitudes. For precipitation, we first created a monthly  
19 climatology from the daily record (1979-1981) and then scaled the daily WFDEI precipitation by  
20 maintaining the monthly climatology value (Lawrence and Slater, 2010):

$$21 \quad P'(y, m, d) = \frac{\overline{P(m)}}{P(y, m)} P(y, m, d) \quad (1)$$

22 where  $y$ ,  $m$  and  $d$  represent a particular year, month and day;  $\overline{P(m)}$  is the precipitation monthly  
23 climatology averaged from 1979 to 1981 and  $P(y, m)$  is the monthly total precipitation for a  
24 particular year and month;  $P(y, m, d)$  and  $P'(y, m, d)$  are the original and scaled daily  
25 precipitation for a particular year, month and day, respectively. Due to a relatively short record  
26 (i.e. 1979-1981) and large variability in northern latitude precipitation, the ratio of  $\frac{\overline{P(m)}}{P(y, m)}$  may  
27 be too large for a particular month with very low precipitation rates. In this case, the daily

1 precipitation was not adjusted to avoid unreasonable estimates. We then ran the model with  
2 different configurations of the daily surface meteorology datasets. Model simulations derived  
3 using the dynamic WFDEI daily surface meteorology from 1979 to 2010 (i.e. varying T and P)  
4 was used as the model baseline simulation. For the temperature sensitivity analysis, we ran the  
5 model using the dynamic daily WFDEI temperature records from 1979 to 2010, but holding P as  
6 the climatology value from 1979-1981. For the precipitation sensitivity analysis, we ran the  
7 model using the dynamic daily WFDEI precipitation records, but with the T daily climatology.  
8 Since VPD is dependent on air temperature, we also created a daily VPD climatology (1979-  
9 1981) as an additional input to the carbon model, assuming negligible changes in relative  
10 humidity during the study period for the precipitation sensitivity analysis. There was no  
11 significant trend in solar radiation during the study period; we therefore used the historical (i.e.  
12 1979-2010) solar radiation data for the three sets of simulations.

13 The model was initialized using a two-step process prior to the three sets of simulations. The  
14 model was first spun-up using the daily surface climatology (1979-1981) including T, VPD, and  
15 P for 50 years to bring the top 3-m soil temperature into dynamic equilibrium; the model was  
16 then run using the same climatology and simulated soil temperature and moisture fields over  
17 several thousand years to bring the SOC pools to equilibrium.

18 We mainly used correlation analysis to evaluate the climatic controls on simulated soil  
19 temperature and carbon fluxes. The outputs from the model baseline simulations (i.e. varying T  
20 and P) from 1982 to 2010 were used for this analysis. The period from 1979 to 1981 was  
21 excluded in order to reduce the impact of the spin-up process on model simulations. We first  
22 calculated the correlation coefficients between the time series of each climate variable and  
23 modeled soil temperature or carbon fluxes at each grid cell from 1982 to 2010. The resulting  
24 correlation coefficients were then averaged for each climate zone classified using the annual  
25 mean air temperature (1982-2010) and binned into 2.5 °C intervals. The climate variables used in  
26 the correlation analysis included air temperature, snow water equivalent (SWE) and snow cover  
27 extent (SCE). The model did not simulate SCE directly, and the SCE was estimated using the  
28 following equation:

$$29 \quad SCE = \frac{SNOWD}{0.1 + SNOWD} \quad (2)$$

1 where *SNOWD* is the simulated snow depth (m), and the surface roughness was set as 0.1 m  
2 (Lawrence and Slater, 2010).

3

### 4 **3 Results**

#### 5 **3.1 Model validation**

6 The model simulations were generally consistent with observed daily carbon fluxes from the 20  
7 EC tower sites across the pan-Arctic domain (Table 2), with mean R values of  $0.84 \pm 0.11$  (SD)  
8 for GPP and  $0.63 \pm 0.17$  for NEE, and mean RMSE differences of  $1.44 \pm 0.50 \text{ gC m}^{-2} \text{ d}^{-1}$  for GPP  
9 and  $1.04 \pm 0.36 \text{ gC m}^{-2} \text{ d}^{-1}$  for NEE. The model results showed relatively large discrepancies with  
10 the tower based carbon fluxes for tundra sites; however, large uncertainties are associated with  
11 the tower measurements in tundra areas due to the characteristically harsh environment and  
12 extensive missing data. The simulated temperature and moisture fields also capture the  
13 seasonality of the in situ surface ( $\leq 15$  cm) soil measurements representing variable soil depths  
14 (not shown), despite large uncertainties in the surface meteorology inputs (particularly  
15 precipitation/snowfall), and soil parameters including definition of texture and peat fraction  
16 within the soil profile. Additional assessment of the model simulations was conducted using  
17 detailed in situ measurements at selected tundra and boreal forest validation sites (Table 1) as  
18 summarized below.

19 The model simulations compared favourably with in situ measurements at the tundra validation  
20 sites for surface soil temperature ( $R=0.93$ ,  $\text{RMSE}=3.12^\circ\text{C}$ ) and carbon fluxes, including GPP  
21 ( $R=0.72$ ,  $\text{RMSE}=0.76 \text{ gC m}^{-2} \text{ d}^{-1}$ ) and NEE ( $R=0.79$ ,  $\text{RMSE}=0.50 \text{ gC m}^{-2} \text{ d}^{-1}$ ), but with relatively  
22 larger discrepancy during the winter when the model showed lower values of NEE (e.g., less  
23  $\text{CO}_2$  emissions) than the measurements (December to February, DJF; Fig. 1). The simulated  
24 maximum soil thaw depth ( $\sim 50$  cm averaged from 2008 to 2011) was also consistent with site  
25 measurements, ranging from 40 to 70 cm at three locations within the tundra validation site  
26 (Euskirchen et al., 2012). An apparent cold bias ranging from  $-2$  to  $-5^\circ\text{C}$  in the simulated soil  
27 temperature during the fall and winter period of year 2009 and 2010 (Fig.1a) reflects lower  
28 model simulated snow depth and associated reductions in thermal buffering between the  
29 atmosphere and underlying soil layers. This cold bias in the simulated soil temperatures results in

1 early freezing of simulated soil water content (Fig. S4). Compared with the tower observations,  
2 the simulated daily surface soil temperatures generally show large temporal variations,  
3 particularly during the summer (June to August, JJA). There were also considerable differences  
4 among in situ soil temperatures at the different tundra sites. Summer (JJA) soil temperature at the  
5 wet sedge tundra location was generally lower than the other tundra vegetation types, which may  
6 reflect higher soil water content and specific heat capacity, and greater latent heat loss from  
7 evapotranspiration, leading to slower soil warming at this site. Overall, the model simulations  
8 compare well with the tower observed carbon fluxes during the growing season, but significantly  
9 underestimate NEE and soil respiration during the dormant season. Model underestimation of  
10 soil respiration during the dormant season may reflect less liquid soil water represented by the  
11 model under frozen ( $<0^{\circ}\text{C}$ ) temperatures than the tower measurements (Fig. S4), and also a lack  
12 of model representation of wind-induced  $\text{CO}_2$  exchange between the atmosphere and surface  
13 snow pack (Luers et al., 2014). The model generally shows earlier seasonal onset and offset of  
14 photosynthesis relative to the in situ measurements, while partitioning of the tower NEE  
15 measurements during the shoulder season may be subject to large uncertainties under partial  
16 snow cover conditions (Euskirchen et al., 2012).

17 The model simulations also compared favourably against observations at the boreal forest  
18 validation sites (Fig. 2), capturing observed seasonality in soil temperatures ( $R>0.95$ ,  
19  $\text{RMSE}<2.00^{\circ}\text{C}$ ) at different soil depths, and daily variations in tower observed carbon fluxes for  
20 GPP ( $R=0.89$ ,  $\text{RMSE}=1.24 \text{ gC m}^{-2} \text{ d}^{-1}$ ) and NEE ( $R=0.73$ ,  $\text{RMSE}=0.65 \text{ gC m}^{-2} \text{ d}^{-1}$ ). Similar to  
21 the tundra sites, snow depth also has a large impact on simulated soil temperatures at the boreal  
22 forest sites, but is subject to large uncertainties from both model snowfall inputs and forest  
23 canopy snow interception processes. The timing of simulated thaw and freeze of soil water at  
24 different depths is generally consistent with the tower measurements, with later seasonal thawing  
25 and freezing occurring in deeper soils (Fig. S5). The tower site soil moisture measurements show  
26 larger variability than the model simulations during the growing season, which likely reflect  
27 differences in the model parameterization of surface moss/peat and mineral soil hydraulic  
28 conductivities relative to local site conditions. The model simulated NEE fluxes during the non-  
29 growing season stem mainly from soil heterotrophic respiration and are largely consistent with  
30 the in situ tower observations, generally diminishing towards the end of the year, and then  
31 gradually recovering with soil warming toward the onset of the growing season. Both the model

1 and in situ tower NEE fluxes show large temporal variations during the growing season, largely  
2 due to GPP reductions caused by high vapour pressure deficits or water stress.

3 The model simulated SCE was generally consistent with satellite observation based global  
4 climate data records documenting weekly SCE changes (Brown and Robinson, 2011; Fig. 3).  
5 The model simulations show a similar mean seasonal cycle as the satellite observations, with  
6 spring snow melt mostly occurring from April to May, and fall onset of seasonal snow cover  
7 occurring in October over the 1982 to 2010 record (Fig. 3a). The model simulated SCE shows  
8 consistent changes with the satellite observations in spring, indicating realistic simulation of the  
9 snow melting process. However, the model generally underestimates SCE in the fall and winter.  
10 The model did not directly simulate SCE, which was calculated from simulated snow depth  
11 using an empirical equation (Eq. 2). Based on Eq.2, the modelled SCE will never approach 100  
12 percent, while the satellite data indicates nearly complete winter snow cover over the study  
13 domain. Larger model SCE differences from the satellite observations are expected when the  
14 snow cover is relatively shallow and patchy owing to the relatively coarse spatial resolution of  
15 both model simulations and satellite observations. Moreover, the satellite SCE dataset is  
16 presented as a binary classification at a weekly time step, which may not adequately depict  
17 transient SCE fluctuations under active surface melting and freezing processes in the fall (Kim et  
18 al., 2015).

### 19 **3.2 Climatic control on simulated permafrost and soil temperatures**

20 The simulated permafrost area is generally consistent with reported estimates from previous  
21 studies. The simulated mean permafrost area from 1982 to 2010 is approximately 11.3 million  
22 km<sup>2</sup>, which is within the range of observation based estimates (11.2-13.5 million km<sup>2</sup>) of the  
23 combined area for continuous (90-100%) and discontinuous (50-90%) permafrost extent over the  
24 northern polar region ( $\geq 45^{\circ}\text{N}$ ) (Zhang et al., 2000).

25 The simulated active layer depth (ALD) shows an overall increasing trend across the pan-Arctic  
26 domain over the 1982 to 2010 record (Fig. 4a, b). No strong bias was observed for the model  
27 ALD simulations compared against in situ observations for 53 pan-Arctic sites from the  
28 Circumpolar Active Layer Monitoring (CALM) program (Brown et al., 2000); these results  
29 showed a mean model bias of -9.48 cm, representing approximately 16.5% of the estimated ALD,

1 but with low model correspondence ( $R=0.31$ ,  $p<0.1$ ) relative to in situ site observations (Fig. S6).  
2 The discrepancy between model simulated ALD results and in situ observations may be partly  
3 due to a spatial scale mismatch between the coarse resolution model simulations and the local  
4 CALM site measurements, as well as uncertainties in the reanalysis surface meteorology data  
5 used as model forcings (Rawlins et al., 2013). Previous studies have shown large local spatial  
6 variations in ALD due to strong surface heterogeneity including microtopography, vegetation  
7 and soil moisture conditions (Romanovsky et al., 2010 a, b; Mishra and Riley, 2014). Simulated  
8 widespread ALD deepening is consistent with generally decreasing snow cover extent in the pan-  
9 Arctic region (Fig. 4c). Simulated ALD trends over the 1982-2010 record range from  $-4.32$  cm  
10  $\text{yr}^{-1}$  to  $8.05$  cm  $\text{yr}^{-1}$ , with a mean value of  $0.66$  cm  $\text{yr}^{-1}$ . A notable model ALD deepening trend  
11 occurs in discontinuous permafrost areas with relatively large mean ALD values. However, in  
12 portions of Alaska, the model simulations indicate slightly decreasing ALD trends across the  
13 study period (Fig. 4b), despite strong reduction in the local snow cover extent (Fig. 4c). This  
14 mainly reflects a large decrease in the simulated snowpack (Fig. 4d) due to a decreasing trend in  
15 WFDEI precipitation/snowfall data, resulting in less thermal insulation of underlying soil, which  
16 may offset warming effects from decreasing snow cover extent.

17 The regional differences in snow cover effects on model simulated ALD can be explained by  
18 different climatic controls on warm-season (May to October) soil temperatures. The correlation  
19 analysis between climate variables and warm-season soil temperatures (Fig. 5) indicates that  
20 surface warming has a dominant control on upper ( $<0.5$  m) soil temperatures in all climate zones,  
21 and also on deeper ( $\geq 0.5$  m) soil temperatures in warmer climate zones (mean annual  $T_{\text{air}} > -4^{\circ}\text{C}$ ).  
22 A deep snow pack has a strong warming effect on simulated deeper ( $\geq 0.5$  m) soil temperatures in  
23 colder climate zones (mean annual  $T_{\text{air}} \leq -4^{\circ}\text{C}$ ), but with limited warming effects on surface soil  
24 temperatures across all pan-Arctic climate zones. Correspondingly, the effects of seasonal snow  
25 cover duration on model soil temperatures vary across different climate zones and soil depths. In  
26 colder climate areas, a longer snow cover duration has a relatively strong warming effect on  
27 deeper ( $\geq 0.5$  m) soil temperatures, but with negligible warming effects on surface soil layers. In  
28 warmer areas, a shorter snow cover season promotes warmer soils, particularly within surface  
29 soil layers, due to stronger air and soil thermal coupling. Additional analysis also indicates that  
30 earlier snow cover seasonal onset in the fall has a stronger warming effect on modelled soil

1 temperatures in colder climate areas, while earlier offset of seasonal snow cover in the spring has  
2 a stronger warming effect on modelled soil temperatures in warmer climate areas.

### 3 **3.3 Climatic control on simulated carbon fluxes**

4 The model simulations indicated that air temperature has an overall dominant control on the two  
5 main components of the NEE flux (i.e. NPP and Rh) across all pan-Arctic climate zones, while  
6 snow has a larger control on estimated annual NEE fluxes in colder climate areas (Fig. 6). These  
7 results indicate that warming generally promotes vegetation photosynthesis and soil  
8 heterotrophic respiration in the pan-Arctic region. However, a reduced positive correlation  
9 between NPP and air temperature in warmer climate zones (mean  $T_{air} > 0^{\circ}\text{C}$ ) also indicates that  
10 warming-induced drought may reduce vegetation productivity to some extent (Kim et al., 2012;  
11 Yi et al., 2014). No significant correlation ( $p > 0.1$ ) between NEE and air temperature was  
12 observed for most areas (mean  $T_{air} \leq 5^{\circ}\text{C}$ ) due to NEE being a residual between two large fluxes  
13 (i.e. NPP and Rh) with similar temperature responses. A predominantly positive correlation  
14 (mean  $R = 0.32$ ;  $p < 0.1$ ) between annual NEE and SWE in colder regions (mean  $T_{air} < -4^{\circ}\text{C}$ ) is  
15 mainly due to a strong positive correlation ( $R > 0.60$ ,  $p < 0.01$ ) between SWE and NEE fluxes  
16 during the cold season (November to April; Fig. S7). A deeper snow pack promotes warmer soil  
17 conditions (Fig. 5b) and associated SOC decomposition and heterotrophic respiration, which  
18 contributes significantly to annual NEE, especially in colder climate areas (Zimov et al., 1996).  
19 No significant correlation ( $p > 0.1$ ) between annual SCE/SWE and warm-season (MJJASO)  
20 carbon fluxes was observed.

21 While snow cover has a negligible effect on total estimated carbon fluxes during the warm  
22 season, it has a strong control on the composition of soil Rh (Fig. 7). An overall, deeper snow  
23 pack promotes soil decomposition and respiration from deeper ( $\geq 0.5$  m) soil layers, while  
24 inhibiting contributions from surface ( $\leq 0.2$  m) soil layers, especially in colder climate areas. This  
25 response is due to a stronger warming effect of snow cover on deeper soil layers in colder areas  
26 (Fig. 5). Comparatively, even though air temperature has a strong control on total warm-season  
27 Rh fluxes, it has a limited effect on the contribution of different soil depths to total soil  
28 decomposition and respiration except in the warmer climate areas (mean annual  $T_{air} > 0^{\circ}\text{C}$ ). In  
29 the cold season, a deeper snow pack also promotes soil decomposition in deeper ( $> 0.2$  m) soil  
30 layers more than in surface (0-0.2 m) soil layers.

### 1 **3.4 Sensitivity of simulated soil thermal dynamics and soil carbon decomposition** 2 **to climate variations**

3 The model sensitivity analysis using different surface meteorology inputs indicated that warming  
4 and reduced snow cover extent promoted widespread ALD deepening across the pan-Arctic  
5 domain over the 1982 to 2010 record (Fig. 8). In Eurasia, strong winter warming reduced model  
6 simulated SWE and SCE, while increasing winter precipitation generally increased SWE and  
7 SCE. In North America, regional trends in winter snow pack and SCE were more variable due to  
8 variable trends in winter air temperature and precipitation. Therefore, the resulting model  
9 simulated trends in SWE and SCE based on varying temperature and precipitation inputs showed  
10 strong spatial heterogeneity across the pan-Arctic domain. The model sensitivity analysis based  
11 on varying temperature inputs alone indicated overall ALD deepening in permafrost areas,  
12 corresponding with widespread warming and reduced SCE. However, the sensitivity analysis  
13 based on varying precipitation alone showed more variable trends in the simulated ALD results.  
14 Areas with strong decreasing winter precipitation and snow pack trends, such as interior Alaska  
15 and eastern Siberia, showed a decreasing ALD trend, attributed to reduced snow insulation  
16 effects. The results also indicated that changing air temperature had an overall dominant effect  
17 on the simulated ALD trends, though changing precipitation also contributed to ALD changes in  
18 some areas.

19 The model sensitivity analysis indicated that varying precipitation accounts for more of the  
20 change in the simulated Rh contribution from different soil depths (i.e., soil Rh fraction, Figs. 9  
21 and 10, and Fig. S8), which is consistent with the above results indicating strong control of snow  
22 cover on the soil Rh fraction at different soil depths. The model sensitivity results also indicated  
23 that changing air temperature has minimal impact on the simulated soil Rh fraction, while  
24 increasing (decreasing) winter snow pack in permafrost areas generally corresponded with  
25 increasing (decreasing) soil Rh fraction from deeper (>0.5 m) soil layers and decreasing  
26 (increasing) soil Rh contributions from surface (0-0.2 m) soil layers (Fig. 9). This is particularly  
27 true in cold climate regions (mean annual  $T_{air} < -10^{\circ}\text{C}$ ; Fig. 10). The simulated Rh fraction from  
28 the deeper soil layers (0.5-3.0 m) based on model runs using varying precipitation alone did not  
29 show significant differences ( $p > 0.1$ ) from model simulations based on varying air temperature  
30 and precipitation. However, the simulated soil Rh fraction from both surface (0-0.2 m) and  
31 deeper (0.5-3.0 m) soil layers based on model runs using varying temperature alone was



1 significantly ( $p < 0.01$ ) different from model simulation results based on varying air temperature  
2 and precipitation. Moreover, cold regions (mean  $T_{air} < -10^{\circ}\text{C}$ ) showed stronger decreasing trends  
3 in the Rh fraction from surface soil layers and increasing soil Rh contributions from deeper soil  
4 layers, likely due to increasing winter precipitation and snow cover (Figs. 8 and 9), and  
5 consistent with field studies involving snow cover manipulations and associated impacts on soil  
6 respiration (e.g. Nowinski et al., 2010).

7

## 8 **4 Discussion**

### 9 **4.1 Impact of climate variations on soil active layer properties**

10 Our results show that recent strong surface warming trends in the pan-Arctic region have  
11 promoted widespread soil thawing and active layer (ALD) deepening (Fig. 8), while changing  
12 precipitation and snow depth have had a relatively smaller impact on ALD trends (Figs. 4 and 8).  
13 We find a mean increasing ALD trend of  $0.66 \pm 1.20 \text{ cm yr}^{-1}$  across the pan-Arctic region over the  
14 past three decades, which is similar to reported values from previous studies (Zhang et al., 2005;  
15 Romanovsky et al., 2010a), albeit representing different time periods. This overall ALD  
16 deepening trend across the pan-Arctic domain corresponds with widespread warming and  
17 warming-induced decreases in SCE (Fig. 4c), and increasing non-frozen season duration (Kim et  
18 al., 2012). Our analysis indicates that air temperature has a dominant control on upper ( $< 0.5 \text{ m}$ )  
19 soil layer temperatures during the warm-season, with increasing control in warmer climate zones  
20 (Fig. 5a). The model simulations also suggest that most pan-Arctic permafrost areas, especially  
21 continuous permafrost areas, have a relatively shallow ( $< 1 \text{ m}$ ) active layer (e.g. Fig. 4a).  
22 Therefore, rapid warming of the upper soil layers corresponds with general ALD deepening.

23 Previous studies have also shown that summer air temperature is a primary control on ALD  
24 trends, while the relationship between snow cover and ALD is more variable (Zhang et al., 2005;  
25 Romanovsky et al., 2010a, b). Our results demonstrate that deeper snow pack conditions promote  
26 warming of deep ( $> 0.5 \text{ m}$ ) soil layers, especially in colder climate areas (Fig. 5b), and this effect  
27 exceeds the impact of surface warming on deeper soil layers (e.g.  $> 1 \text{ m}$ ). Previous studies  
28 indicate that changes in snow depth can influence borehole (10-20 m) permafrost temperatures as  
29 much as changes in air temperature (Stieglitz et al., 2003; Romanovsky et al., 2010a, b).

1 Regional simulations from the improved Community Land Model (CLM) also indicate that snow  
2 state changes can explain 50% or more of soil temperature trends at 1m depth over the recent 50  
3 year record (Lawrence and Slater, 2010). On the other hand, the impact of changing snow cover  
4 duration on soil temperatures may vary across different climate zones (Fig. 5c) due to the  
5 influence of both precipitation/snowfall and air temperature on snow cover duration. A shorter  
6 snow cover season may cool the soil in colder climate zones due to less insulation from cold  
7 temperatures, but may warm the soil in warmer climate zones by promoting greater atmospheric  
8 heat transfer into soils (Lawrence and Slater, 2010; Euskirchen et al., 2007). Our results indicate  
9 that recent regional trends toward continued warming, earlier spring snowmelt onset and a  
10 shorter snow cover season will likely enhance soil warming and permafrost degradation in  
11 relatively warmer (mean annual  $T_{air} > -5^{\circ}\text{C}$ ) regions of the pan-Arctic domain.

## 12 **4.2 Impact of climate variations on soil carbon dynamics**

13 Snow cover is an important control on the annual carbon budget in cold regions (annual mean  
14  $T_{air} < -4^{\circ}\text{C}$ ; Fig. 6b-c), even though air temperature has a dominant control on both annual NPP  
15 and Rh fluxes across all climate zones (Fig. 6a). Strong snow cover buffering of underlying soil  
16 temperatures sustains soil respiration even under very cold winter air temperatures and the  
17 resulting winter soil respiration can be a large component of the annual NEE budget (Sullivan et  
18 al., 2010). Field experiments have shown that winter soil respiration in tundra areas can offset  
19 total net carbon uptake during the growing season and thus switch the ecosystem from a net  
20 carbon sink to a carbon source (Zimov et al., 1996; Euskirchen et al., 2012; Luers et al., 2014).  
21 Our results also indicate that cold-season (November-April) Rh accounts for ~25% of total  
22 annual Rh over the entire pan-Arctic domain, while this estimate may be conservative since our  
23 model may underestimate soil respiration in tundra areas (Fig. 1b). The model simulations  
24 indicate very low (<5%) unfrozen water below  $\sim -3^{\circ}\text{C}$  at the tundra sites, while previous studies  
25 and the tower measurements (Fig. S4) indicate that substantial unfrozen water may remain even  
26 under very low soil temperatures (e.g.  $\sim -10^{\circ}\text{C}$ ), sustaining soil microbial activities (Romanovsky  
27 and Osterkamp, 2000). On the other hand, winter warming may change the depth and structure of  
28 insulating snow cover, affecting underlying soil temperatures, which could alter soil N  
29 mineralization rates and soil microbial activities that influence ecological processes during the  
30 growing season (Schimel et al., 2004; Sturm et al., 2005; Monson et al., 2006).

1 Even though air temperature has a dominant control on Rh during the warm season (from May to  
2 October), snow cover strongly influences the contribution of different soil depths to total soil  
3 decomposition and Rh (Fig. 7). This non-linear response is due to different controls of surface air  
4 temperature and snow cover on soil temperatures at different soil depths (Zhang, 2005;  
5 Romanovsky et al., 2010a, b; Lawrence and Slater, 2010). Surface warming during the summer  
6 has a dominant control on upper soil layer temperatures (<0.5 m; Fig. 5a), while a deeper winter  
7 snowpack has a persistent warming effect on deeper soil temperatures in colder climate areas  
8 (Fig. 5b; Gouttevin et al., 2012). Therefore, surface warming likely promotes more heterotrophic  
9 respiration from surface litter and soil layers, while a deeper snow pack promotes soil respiration  
10 from deeper soil layers. This is particularly important for soil carbon dynamics in permafrost  
11 areas, where a large amount of soil carbon occurs in deep perennial frozen soils (Hugelius et al.,  
12 2014). Previous studies including field experiments have primarily focused on the effects of  
13 surface warming on permafrost soil carbon decomposition (e.g. Schuur et al., 2007; Koven et al.,  
14 2011; Schaefer et al., 2011), while our results show that snow cover may play a larger role than  
15 air temperature in influencing deeper soil temperatures and permafrost stability. This is also  
16 supported by a recent snow addition experiment in Alaska tundra areas (Nowinski et al., 2010),  
17 which showed that a deeper snow treatment resulted in a larger contribution of deep and old soil  
18 carbon decomposition to total soil heterotrophic respiration.

### 19 **4.3 Limitations and uncertainties**

20 Although soil temperature and moisture are the two major environmental controls on soil carbon  
21 decomposition, other factors may also influence soil decomposition rates and permafrost carbon  
22 feedback potential, but not represented by our modeling study (Hobbie et al., 2000). A number of  
23 chemical and biological factors can affect the temperature sensitivity of soil carbon  
24 decomposition in northern soils, including enzyme abundance, microbial population size and  
25 oxygen availability (Waldrop et al., 2010). Previous studies also show that soil carbon  
26 decomposition rates may be depth-dependent. Accounting for vertical changes in soil  
27 biogeochemical properties and processes, including the size and substrate quality of the soil  
28 active layer and permafrost carbon pool, and the degree of N mineralization with decomposing  
29 permafrost carbon, may have significant impacts on the sign and magnitude of the projected  
30 high-latitude carbon response to future warming (Koven et al., 2011; Koven et al., 2015). Finally,

1 changing wintertime soil microclimate will alter the amount and timing of plant-available  
2 nutrients (N) in tundra ecosystems, and may drive a positive feedback between snow, soil  
3 temperature, microbial activity, and plant community composition (Schimel et al., 2004; Sturm  
4 et al., 2005).

5 A number of processes, notably fire disturbance, shrub expansion and thermokarst, are not  
6 included in this study but may be important factors affecting regional permafrost and soil carbon  
7 dynamics (Grosse et al., 2011; Schuur et al., 2015). A warming climate has been linked with  
8 increasing boreal-arctic fire activity and severity (Grosse et al., 2011). Fire can change the  
9 surface vegetation composition and consume a large portion of the soil organic layer, which can  
10 dramatically alter the surface energy balance and soil thermal properties, and cause rapid  
11 permafrost degradation (Harden et al. 2006; Jafarov et al., 2013). Both field experiments and  
12 satellite measurements indicate a “greening” Arctic with increasing shrub abundance due to  
13 climate warming (Tape et al., 2006). Shrub expansion in Arctic tundra can change the snow  
14 distribution and surface albedo, affecting the surface energy balance and underlying active layer  
15 and permafrost conditions (Sturm et al., 2005). Development of surface water ponding with  
16 thermokarst in ice-rich permafrost areas can alter the local surface hydrology, affecting  
17 permafrost and soil carbon decomposition (Schuur et al., 2007; Grosse et al., 2011).

18 Another important feature of the Arctic is strong surface heterogeneity, characterized by  
19 widespread lakes, ponds, wetlands and waterlogged soils as a result of both topography and  
20 restricted surface drainage due to underlying permafrost. Changes in both surface and subsurface  
21 hydrology are tightly coupled with local permafrost conditions and potential carbon and climate  
22 feedbacks (Smith et al., 2005; Watts et al., 2012; Yi et al., 2014; Schuur et al., 2015). Current  
23 large-scale model simulations, including this study, generally operate at the order of tens of  
24 kilometers or even larger, and may not adequately represent the effects of surface heterogeneity  
25 on simulated permafrost hydrologic processes and soil carbon decomposition processes (Koven  
26 et al., 2011; Rawlins et al., 2013; Schuur et al., 2015). For example, most models prescribe a  
27 dominant vegetation type or a single value for the organic layer thickness commensurate with the  
28 model spatial resolution, which likely introduces large uncertainties to the model simulated  
29 moisture and heat fluxes and thus the permafrost properties. Next generation satellites, including  
30 the NASA SMAP (Soil Moisture Active Passive) mission provide for finer-scale (i.e. 3-9 km  
31 resolution) monitoring and enhanced (L-band) microwave sensitivity to surface (~<5 cm) soil

1 freeze/thaw and moisture conditions (Entekhabi et al., 2010), and may enable improved regional  
2 hydrological and ecological model parameterizations and simulations that more accurately  
3 represent active layer conditions. Finer spatial scale observations using lower frequency (such as  
4 P-band) Synthetic Aperture Radar (SAR) measurements from airborne sensors such as AirMOSS  
5 (Tabatabaenejad et al., 2015) may also provide improved information on sub-grid scale  
6 processes and subsurface soil thermal and moisture profiles, providing critical constraints on  
7 model predictions of soil active layer changes, and soil carbon and permafrost vulnerability.

8

## 9 **5 Conclusions**

10 We developed a coupled hydrology and terrestrial carbon flux modeling framework to evaluate  
11 the sensitivity of soil thermal and carbon dynamics to snow cover and recent climate variations  
12 across the pan-Arctic basin and Alaska during the past 3 decades (1982-2010). Our results  
13 indicate that surface warming promotes wide-spread soil thawing and active layer deepening due  
14 to strong control of surface air temperature on upper ( $<0.5$  m) soil temperatures during the warm  
15 season (from May to October). Recent trends indicating earlier spring snowmelt and shorter  
16 seasonal snow cover duration with regional warming (Dyer and Mote, 2006; Brown and  
17 Robinson, 2011; Kim et al., 2012) will most likely enhance soil warming in relatively warmer  
18 climate zones (mean annual  $T_{air} > -5^{\circ}\text{C}$ ) and promote permafrost degradation in these areas. Even  
19 though air temperature has a dominant control on soil decomposition during the warm season,  
20 snow cover has a strong control on the contribution of different soil depths to the total soil  
21 heterotrophic respiration flux. A deeper snow pack inhibits surface ( $<0.2$  m) litter and soil  
22 organic carbon decomposition, but enhances soil decomposition and respiration from the deeper  
23 ( $>0.5$  m) soil carbon pool. This non-linear relationship between snow cover and soil  
24 decomposition is particularly important in permafrost areas, where a large amount of soil carbon  
25 is stored in deep perennial frozen soils that are potentially vulnerable to mobilization and  
26 accelerated losses from near-term climate change. Our results demonstrate the important control  
27 of snow cover in affecting active layer properties and soil carbon decomposition processes across  
28 the pan-Arctic, and the necessity of considering both warming, and changing precipitation and  
29 snow cover regimes in characterizing permafrost soil carbon dynamics. In addition, further  
30 improvements in regional assessment and monitoring of precipitation and snow cover across the

1 northern high latitudes are needed to improve quantification and understanding of linkages  
 2 between snow and permafrost carbon dynamics.

3

## 4 **Appendix**

### 5 **A1 Hydrology model description**

6 The PWBM model (Rawlins et al., 2013) simulates snow and ground thermal dynamics by  
 7 solving a 1-D heat transfer equation with phase change (Nicolosky et al., 2007):

$$8 \quad C \frac{\partial}{\partial t} T(z, t) + L \zeta \frac{\partial}{\partial t} \theta(T, z) = \frac{\partial}{\partial z} \left( \lambda \frac{\partial}{\partial z} T(z, t) \right), \quad (A1)$$

9  $z \in [z_s, z_b]$

10 where  $T(z, t)$  is the temperature ( $^{\circ}\text{C}$ ),  $C(T, z)$  and  $\lambda(T, z)$  are the volumetric heat capacity ( $\text{J m}^{-3}$   
 11  $\text{K}^{-1}$ ) and thermal conductivity ( $\text{W m}^{-1} \text{K}^{-1}$ ) of soil respectively;  $L$  is the volumetric latent heat of  
 12 fusion of water ( $\text{J m}^{-3}$ );  $\zeta$  is the volumetric water content, and  $\theta$  is the unfrozen liquid water  
 13 fraction. The Dirichlet boundary conditions at the snow/ground surface  $z_s$ , i.e.,  $T(z_s, t) = T_{air}(t)$ ,  
 14 and a heat boundary condition at the lower boundary  $z_b$ , i.e.,  $\lambda \frac{\partial}{\partial z} T(l, t) = g$ , were used to solve  
 15 the heat equation, where  $T_{air}$  is the observed air temperature and  $g$  is the geothermal heat flux ( $\text{K}$   
 16  $\text{m}^{-1}$ ). The volumetric water content ( $\zeta$ ) can be obtained by solving the Richard's equation. The  
 17 unfrozen liquid water fraction ( $\theta$ ) was estimated empirically as:

$$17 \quad \theta = \begin{cases} 1 & T \geq T_* \\ |T_*|^b |T|^{-b} & T < T_* \end{cases} \quad (A2)$$

18 where the constant  $T_*$  is the freezing point depression, and  $b$  is a dimensionless parameter  
 19 obtained from unfrozen water curve fitting (Romanovsky and Osterkamp, 2000).

20 The bulk thermal properties of soil (i.e.  $C$  and  $\lambda$ ) are a combination of the thermal properties of  
 21 soil solids, air, and thawed and frozen states of soil water (Rawlins et al., 2013). Particularly, for  
 22 the soil solids, the volumetric heat capacity ( $C_s$ ) and thermal conductivities ( $\lambda_s$ ) vary with the  
 23 fraction of organic carbon of the soil, defined as:

$$1 \quad C_s = (1-f)C_m + fC_o \quad \lambda_s = \lambda_m^{1-f} \lambda_o^f \quad (A3)$$

2 where  $f$  is the fraction of organic carbon in the soil,  $C_m$  and  $C_o$  are the volumetric heat  
 3 capacities of the mineral and organic soils respectively, and  $\lambda_m$  and  $\lambda_o$  are the thermal  
 4 conductivities of the mineral and organic soils respectively.

5 Up to five snow layers were used to characterize the snowpack dynamics and solve the snow  
 6 temperature profile, with varying depth for each layer depending on the snow depth. A two-layer  
 7 snow density model similar to Schaefer et al. (2009) was used to characterize the impact of the  
 8 bottom depth hoar layer on the snow thermal conductivity for tundra and taiga, with fixed snow  
 9 thermal conductivity for this layer. For the upper snow layer, both the snow heat capacity and  
 10 thermal conductivity vary with snow density. Following Liston et al. (2007), temporal evolution  
 11 of the snow density is mainly affected by new snowfall and compaction due to winds:

$$12 \quad \frac{d\rho_s}{dt} = 0.1a_1U\rho_s e^{(-b(T_f - T_s))} e^{(-a_2\rho_s)} \quad (A4)$$

13 where  $\rho_s$  is the snow density ( $\text{kg m}^{-3}$ ),  $U$  represents the wind-speed contribution to the snow  
 14 density changes with negligible influence for wind speed below 5 m/s;  $T_f$  and  $T_s$  are the freezing  
 15 and snow temperatures, respectively;  $a_1$ ,  $a_2$  and  $b$  are empirical dimensionless parameters. The  
 16 snow thermal conductivity ( $\lambda_{snow}$ ) is an empirical estimate of snow density based on Sturm et al.  
 17 (1997):

$$18 \quad \lambda_{snow} = 0.138 - 1.01\rho_s + 3.233\rho_s^2 \quad (A5)$$

19 More details on the numerical solution of the heat transfer equation and the parametrization of  
 20 the snow model can be found in Rawlins et al. (2013) and Nicolsky et al. (2007).

## 21 **A2 Carbon model description**

22 A satellite-based light use efficiency (LUE) approach was used to estimate vegetation  
 23 productivity:

$$24 \quad GPP = \varepsilon \times FPAR \times PAR \quad (A6)$$

1 where GPP is the gross primary productivity ( $\text{g C m}^{-2} \text{d}^{-1}$ );  $\varepsilon$  ( $\text{g C MJ}^{-1}$ ) is the LUE coefficient  
 2 converting absorbed photosynthetically active solar radiation (APAR) to vegetation biomass, and  
 3 FPAR defines the fraction of incident PAR ( $\text{MJ m}^{-2} \text{d}^{-1}$ ) absorbed by the vegetation canopy (i.e.  
 4 APAR). A maximum LUE coefficient ( $\varepsilon_{mx}$ ,  $\text{g C MJ}^{-1}$ ) was prescribed for each land cover type  
 5 and was reduced for sub-optimal environmental conditions (including low air temperature, soil  
 6 moisture and frozen conditions) to estimate  $\varepsilon$  (Yi et al., 2013). Vegetation net primary  
 7 productivity (NPP) was estimated as a fixed portion of GPP for each biome type based on an  
 8 assumption of conservatism in vegetation carbon use efficiency within similar plant functional  
 9 types.

10 A dynamic carbon allocation of litterfall estimated from NPP, based on Randerson et al. (1996)  
 11 and White et al. (2000), was used to characterize litterfall seasonality. The total litterfall was  
 12 partitioned into three components, including leaves, fine roots, and woody components with  
 13 prescribed ratios for each plant functional type based on field experiments (White et al., 2000;  
 14 Table S2). Daily constant turnover rates were prescribed for the woody components of litterfall  
 15 including stems and coarse roots (White et al., 2000), while the NDVI time series were used to  
 16 characterize turnover rates of the other two variable components of litterfall during leaf  
 17 senescence and active growth periods (Randerson et al., 1996). Approximately half of the fine  
 18 root turnover was assumed to occur during the active growing season, and the monthly variable  
 19 fraction of litterfall was calculated as:

$$\begin{aligned}
 LT_{\text{var1}}(t) &= \frac{LL(t)}{\sum_{t=1}^{12} LL(t)} \cdot (LT_{\text{leaf}} + LT_{\text{root}} \cdot 0.5), \\
 20 \quad LT_{\text{var2}}(t) &= \frac{NDVI(t)}{\sum_{t=1}^{12} NDVI(t)} \cdot LT_{\text{root}} \cdot 0.5, \tag{A7} \\
 LL(t) &= [0.5 \cdot NDVI(t-2) + NDVI(t-1)] - [NDVI(t+1) + 0.5 \cdot NDVI(t+2)]
 \end{aligned}$$

21 where  $LT_{\text{var1}}(t)$  and  $LT_{\text{var2}}(t)$  represent the litterfall fraction associated with leaf loss (i.e.  $LL(t)$ )  
 22 and vegetation active growth, respectively;  $LT_{\text{leaf}}$  and  $LT_{\text{root}}$  are the prescribed fractions of leaf  
 23 and fine root components for each plant functional type, respectively (Table S2). The estimated  
 24 monthly litterfall fraction was then distributed evenly within the month.



1 To account for the contribution of deep soil organic carbon pools to the total heterotrophic  
 2 respiration ( $R_h$ ), we extended the original Terrestrial Carbon Flux (TCF) soil decomposition  
 3 model to incorporate soil organic carbon down to 3 m below surface, and multiple litter and soil  
 4 organic carbon (SOC) pools were used to characterize the progressive decomposition of fresh  
 5 litter to more recalcitrant materials. Following BIOME-BGC (Thornton et al., 2002), the new  
 6 soil decomposition model includes 3 litter pools, 3 SOC pools with relatively fast turnover rates  
 7 and a deep SOC pool with slow turnover rates (Fig. S1). The litterfall carbon inputs were first  
 8 allocated to the 3 litter pools according to the substrate quality of each litterfall component, i.e.  
 9 labile, cellulose and lignin fractions of estimated leaf, fine root, and woody litterfall (Table S3;  
 10 White et al., 2000), and then transferred to the SOC pools through progressive decomposition.  
 11 For each carbon pool ( $C_i$ ), the carbon balance of the decomposition process was defined as:

$$12 \quad \frac{\partial C_i}{\partial t} = R_i + \sum_{j \neq i} (1 - r_j) T_{ji} k_j C_j - k_i C_i \quad (\text{A8})$$

13 where  $R_i$  is the carbon input from litterfall allocated to pool  $i$  (only non-zero for the 3 litter  
 14 pools),  $T_{ji}$  is the fraction of carbon directed from pool  $j$  to pool  $i$  with fraction  $r_j$  lost as  
 15 respiration, and  $k_i$  ( $k_j$ ) is the decomposition rate of carbon pool  $i$  ( $j$ ). The heterotrophic  
 16 respiration ( $R_h$ ) is then computed as the sum of respiration fluxes from the decomposition  
 17 process:

$$18 \quad R_h = \sum_{i=1,7} r_i k_i C_i \quad (\text{A9})$$

19 The soil decomposition rate ( $k_i$ ) for each pool is derived as the product of a theoretical maximum  
 20 rate constant ( $k_{mx,i}$ , Fig. S1) and dimensionless multipliers for soil temperature ( $T_{mult}$ ) and  
 21 moisture ( $W_{mult}$ ) constraints to decomposition under prevailing climate conditions:

$$22 \quad k_i = k_{mx,i} \cdot T_{mult} \cdot W_{mult} \quad (\text{A10})$$

23 where  $T_{mult}$  and  $W_{mult}$  vary between 0 (fully constrained) and 1 (no constraint), as defined in Yi et  
 24 al. (2013).

25

1 **Acknowledgments**

2 This work was supported with funding from the NASA Interdisciplinary Research in Earth  
3 Science program. Data from the Imnavait tundra tower measurement was collected through a  
4 grant from the National Science Foundation Office of Polar Programs, Arctic Observatory  
5 Network. We thank Dr. M. Goulden for providing boreal forest tower measurements in Manitoba,  
6 Canada.

## 1 **References**

- 2 Baldocchi, D.: Breathing of the terrestrial biosphere: lessons learned from a global network of  
3 carbon dioxide flux measurement systems, *Australian Journal of Botany*, 56, 1-26, 2008.
- 4 Bi, J., Xu, L., Samanta, A., Zhu, Z., and Myneni, R.: Divergent Arctic-Boreal Vegetation  
5 Changes between North America and Eurasia over the Past 30 Years, *Remote Sensing*, 5, 2093-  
6 2112, 2013.
- 7 Brown, J., Hinkel, K. M., and Nelson, F. E.: The circumpolar active layer monitoring (CALM)  
8 program: Research designs and initial results, *Polar Geography*, 24, 166-258, 2000.
- 9 Brown, R. D. and Robinson, D. A.: Northern Hemisphere spring snow cover variability and  
10 change over 1922-2010 including an assessment of uncertainty, *Cryosphere*, 5, 219-229, 2011.
- 11 Dyer, J. L. and Mote, T. L.: Spatial variability and trends in observed snow depth over North  
12 America, *Geophys. Res. Lett.*, 33, L16503, doi:10.1029/2006GL027258, 2006.
- 13 Entekhabi, D., Njoku, E. G., O'Neill, P. E., Kellogg, K. H., Crow, W. T., Edelstein, W. N., Entin,  
14 J. K., Goodman, S. D., Jackson, T. J., Johnson, J., Kimball, J., Piepmeier, J. R., Koster, R. D.,  
15 Martin, N., McDonald, K. C., Moghaddam, M., Moran, S., Reichle, R., Shi, J. C., Spencer, M.  
16 W., Thurman, S. W., Tsang, L., and Van Zyl, J.: The Soil Moisture Active Passive (SMAP)  
17 Mission, *P. IEEE*, 98, 704-716, 2010.
- 18 Euskirchen, E. S., Bret-Harte, M. S., Scott, G. J., Edgar, C., and Shaver, G. R.: Seasonal patterns  
19 of carbon dioxide and water fluxes in three representative tundra ecosystems in northern Alaska,  
20 *Ecosphere*, 3, 4, doi:10.1890/es11-00202.1, 2012.
- 21 Euskirchen, E. S., McGuire, A. D., and Chapin, F. S.: Energy feedbacks of northern high-latitude  
22 ecosystems to the climate system due to reduced snow cover during 20th century warming,  
23 *Global Change Biology*, 13, 2425-2438, 2007.
- 24 Friedl, M. A., Sulla-Menashe, D., Tan, B., Schneider, A., Ramankutty, N., Sibley, A., and Huang,  
25 X.: MODIS Collection 5 global land cover: Algorithm refinements and characterization of new  
26 datasets, *Remote Sens Environ*, 114, 168-182, 2010.
- 27 Global Soil Data Task. 2000. Global Soil Data Products CD-ROM (IGBP-DIS). CD-ROM.  
28 International Geosphere-Biosphere Programme, Data and Information System, Potsdam,

1 Germany. Available from Oak Ridge National Laboratory Distributed Active Archive Center,  
2 Oak Ridge, Tennessee, U.S.A.

3 Goulden, M. L., McMillan, A. M. S., Winston, G. C., Rocha, A. V., Manies, K. L., Harden, J. W.,  
4 and Bond-Lamberty, B. P.: Patterns of NPP, GPP, respiration, and NEP during boreal forest  
5 succession, *Global Change Biology*, 17, 855-871, 2011.

6 Gouttevin, I., Menegoz, M., Domine, F., Krinner, G., Koven, C., Ciais, P., Tarnocai, C., and  
7 Boike, J.: How the insulating properties of snow affect soil carbon distribution in the continental  
8 pan-Arctic area, *J Geophys Res-Biogeophys*, 117, 2012.

9 Grosse, G., Harden, J., Turetsky, M., McGuire, A. D., Camill, P., Tarnocai, C., Frohling, S.,  
10 Schuur, E. A. G., Jorgenson, T., Marchenko, S., Romanovsky, V., Wickland, K. P., French, N.,  
11 Waldrop, M., Bourgeau-Chavez, L., and Striegl, R. G.: Vulnerability of high-latitude soil organic  
12 carbon in North America to disturbance, *J. Geophys. Res.*, 116, G00K06,  
13 doi:10.1029/2010JG001507, 2011.

14 Harden, J. W., Manies, K. L., Turetsky, M. R., and Neff, J. C.: Effects of wildfire and permafrost  
15 on soil organic matter and soil climate in interior Alaska, *Global Change Biology*, 12, 2391-2403,  
16 2006.

17 Hobbie, S. E., Schimel, J. P., Trumbore, S. E., and Randerson, J. R.: Controls over carbon  
18 storage and turnover in high-latitude soils, *Global Change Biology*, 6, 196-210, 2000.

19 Hugelius, G., Strauss, J., Zubrzycki, S., Harden, J. W., Schuur, E. A. G., Ping, C.-L.,  
20 Schirmer, L., Grosse, G., Michaelson, G. J., Koven, C. D., O'Donnell, J. A., Elberling, B.,  
21 Mishra, U., Camill, P., Yu, Z., Palmtag, J., and Kuhry, P.: Estimated stocks of circumpolar  
22 permafrost carbon with quantified uncertainty ranges and identified data gaps, *Biogeosciences*,  
23 11, 6573-6593, doi:10.5194/bg-11-6573-2014, 2014.

24 Jorgenson, M. T., Shur, Y. L., and Pullman, E. R.: Abrupt increase in permafrost degradation in  
25 Arctic Alaska, *Geophys. Res. Lett.*, 33, L02503, doi:10.1029/2005GL024960, 2006.

26 Kim, Y., Kimball, J. S., Robinson, D. A., and Derksen, C.: New satellite climate data records  
27 indicate strong coupling between recent frozen season changes and snow cover over high  
28 northern latitudes, *Environ. Res. Lett.*, 10, 084004, 2015.

1 Kim, Y., Kimball, J. S., Zhang, K., and McDonald, K. C.: Satellite detection of increasing  
2 Northern Hemisphere non-frozen seasons from 1979 to 2008: Implications for regional  
3 vegetation growth, *Remote Sens Environ*, 121, 472-487, 2012.

4 Kimball, J. S., Jones, L. A., Zhang, K., Heinsch, F. A., McDonald, K. C., and Oechel, W. C.: A  
5 Satellite Approach to Estimate Land-Atmosphere CO<sub>2</sub> Exchange for Boreal and Arctic Biomes  
6 Using MODIS and AMSR-E, *IEEE T Geosci Remote*, 47, 569-587, 2009.

7 Koven, C. D., Lawrence, D. M., and Riley, W. J.: Permafrost carbon–climate feedback is  
8 sensitive to deep soil carbon decomposability but not deep soil nitrogen dynamics, *Proceedings*  
9 *of the National Academy of Sciences*, 201415123, 2015.

10 Koven, C. D., Ringeval, B., Friedlingstein, P., Ciais, P., Cadule, P., Khvorostyanov, D., Krinner,  
11 G., and Tarnocai, C.: Permafrost carbon-climate feedbacks accelerate global warming, *P Natl*  
12 *Acad Sci USA*, 108, 14769-14774, 2011.

13 Jafarov, E. E., Romanovsky, V. E., Genet, H., McGuire, A. D., and Marchenko, S. S.: The  
14 effects of fire on the thermal stability of permafrost in lowland and upland black spruce forests of  
15 interior Alaska in a changing climate, *Environ. Res. Lett.*, 8, 035030, doi:10.1088/1748-  
16 9326/8/3/035030, 2013.

17 Lawrence, D. M. and Slater, A. G.: Incorporating organic soil into a global climate model,  
18 *Climate Dynamics*, 30, 145-160, 2008.

19 Lawrence, D. M. and Slater, A. G.: The contribution of snow condition trends to future ground  
20 climate, *Climate Dynamics*, 34, 969-981, 2010.

21 Liston, G. E., Haehnel, R. B., Sturm, M., Hiemstra, C. A., Berezovskaya, S., and Tabler, R. D.:  
22 Instruments and methods simulating complex snow distributions in windy environments using  
23 SnowTran-3D, *J Glaciol*, 53, 241-256, 2007.

24 Luers, J., Westermann, S., Piel, K., and Boike, J.: Annual CO<sub>2</sub> budget and seasonal CO<sub>2</sub>  
25 exchange signals at a high Arctic permafrost site on Spitsbergen, Svalbard archipelago,  
26 *Biogeosciences*, 11, 6307-6322, 2014.

27 Mishra, U. and Riley, W. J.: Active-Layer Thickness across Alaska: Comparing Observation-  
28 Based Estimates with CMIP5 Earth System Model Predictions, *Soil Science Society of America*  
29 *Journal*, 78, 894, 2014.

- 1 Monson, R. K., Lipson, D. L., Burns, S. P., Turnipseed, A. A., Delany, A. C., Williams, M. W.,  
2 and Schmidt, S. K.: Winter forest soil respiration controlled by climate and microbial community  
3 composition, *Nature*, 439, 711-714, 2006.
- 4 Nicolsky, D. J., Romanovsky, V. E., Alexeev, V. A., and Lawrence, D. M.: Improved modeling  
5 of permafrost dynamics in a GCM land-surface scheme, *Geophys. Res. Lett.*, 34, L08501,  
6 doi:10.1029/2007GL029525, 2007.
- 7 Nowinski, N. S., Taneva, L., Trumbore, S. E., and Welker, J. M.: Decomposition of old organic  
8 matter as a result of deeper active layers in a snow depth manipulation experiment, *Oecologia*,  
9 163, 785-792, 2010.
- 10 Osterkamp, T. E.: Characteristics of the recent warming of permafrost in Alaska, *J. Geophys.*  
11 *Res.-Earth*, 112, F02S02, doi:10.1029/2006JF000578, 2007.
- 12 Park, H., Sherstiukov, A. B., Fedorov, A. N., Polyakov, I. V., and Walsh, J. E.: An observation  
13 based assessment of the influences of air temperature and snow depth on soil temperature in  
14 Russia, *Environ. Res. Lett.*, 9, 064026, doi:10.1088/1748-9326/9/6/064026, 2014.
- 15 Randerson, J. T., Thompson, M. V., Malmstrom, C. M., Field, C. B., and Fung, I. Y.: Substrate  
16 limitations for heterotrophs: Implications for models that estimate the seasonal cycle of  
17 atmospheric CO<sub>2</sub>, *Global Biogeochemical Cycles*, 10, 585-602, 1996.
- 18 Rawlins, M. A., Lammers, R. B., Frolking, S., Fekete, B. z. M., and Vorosmarty, C. J.:  
19 Simulating pan-Arctic runoff with a macro-scale terrestrial water balance model, *Hydrological*  
20 *Processes*, 17, 2521-2539, 2003.
- 21 Rawlins, M. A., Nicolsky, D. J., McDonald, K. C., and Romanovsky, V. E.: Simulating soil  
22 freeze/thaw dynamics with an improved pan-Arctic water balance model, *Journal of Advances in*  
23 *Modeling Earth Systems*, 5, 659-675, 2013.
- 24 Romanovsky, V. E. and Osterkamp, T. E.: Effects of unfrozen water on heat and mass transport  
25 processes in the active layer and permafrost, *Permafrost and Periglacial Processes*, 11, 219-239,  
26 2000.
- 27 Romanovsky, V. E., Drozdov, D. S., Oberman, N. G., Malkova, G. V., Kholodov, A. L.,  
28 Marchenko, S. S., Moskalenko, N. G., Sergeev, D. O., Ukraintseva, N. G., Abramov, A. A.,

1 Gilichinsky, D. A., and Vasiliev, A. A.: Thermal state of permafrost in Russia, *Permafrost and*  
2 *Periglacial Processes*, 21, 136-155, 2010a.

3 Romanovsky, V. E., Smith, S. L., and Christiansen, H. H.: Permafrost thermal state in the polar  
4 Northern Hemisphere during the international polar year 2007-2009: a synthesis, *Permafrost and*  
5 *Periglacial Processes*, 21, 106-116, 2010b.

6 Schimel, J. P., Bilbrough, C., and Welker, J. A.: Increased snow depth affects microbial activity  
7 and nitrogen mineralization in two Arctic tundra communities, *Soil Biol Biochem*, 36, 217-227,  
8 2004.

9 Smith, L. C., Sheng, Y., MacDonald, G. M., and Hinzman, L. D.: Disappearing Arctic lakes,  
10 *Science*, 308, 1429-1429, 2005.

11 Schaefer, K., Zhang, T. J., Bruhwiler, L., and Barrett, A. P.: Amount and timing of permafrost  
12 carbon release in response to climate warming, *Tellus Series B-Chemical and Physical*  
13 *Meteorology*, 63, 165-180, 2011.

14 Schaefer, K., Zhang, T. J., Slater, A. G., Lu, L. X., Etringer, A., and Baker, I.: Improving  
15 simulated soil temperatures and soil freeze/thaw at high-latitude regions in the Simple  
16 Biosphere/Carnegie-Ames-Stanford Approach model, *J. Geophys. Res.-Earth*, 114, F02021,  
17 doi:10.1029/2008JF001125, 2009.

18 Schuur, E. A. G., Crummer, K. G., Vogel, J. G., and Mack, M. C.: Plant species composition and  
19 productivity following permafrost thaw and thermokarst in alaskan tundra, *Ecosystems*, 10, 280-  
20 292, 2007.

21 Schuur, E. A. G., McGuire, A. D., Schädel, C., Grosse, G., Harden, J. W., Hayes, D. J., Hugelius,  
22 G., Koven, C. D., Kuhry, P., Lawrence, D. M., Natali, S. M., Olefeldt, D., Romanovsky, V. E.,  
23 Schaefer, K., Turetsky, M. R., Treat, C. C., and Vonk, J. E.: Climate change and the permafrost  
24 carbon feedback, *Nature*, 520, 171-179, 2015.

25 Serreze, M. C. and Francis, J. A.: The arctic amplification debate, *Climatic Change*, 76, 241-264,  
26 2006.

27 Solomon, S., Intergovernmental Panel on Climate Change., and Intergovernmental Panel on  
28 Climate Change. Working Group I.: Climate change 2007: the physical science basis:

1 contribution of Working Group I to the Fourth Assessment Report of the Intergovernmental  
2 Panel on Climate Change, Cambridge University Press, Cambridge ; New York, 2007.

3 Stieglitz, M.: The role of snow cover in the warming of arctic permafrost, *Geophys. Res. Lett.*,  
4 30, 1721, doi:10.1029/2003GL017337, 2003.

5 Sturm, M., Holmgren, J., Konig, M., and Morris, K.: The thermal conductivity of seasonal snow,  
6 *J Glaciol*, 43, 26-41, 1997.

7 Sturm, M., Schimel, J., Michaelson, G., Welker, J. M., Oberbauer, S. F., Liston, G. E.,  
8 Fahnestock, J., and Romanovsky, V. E.: Winter biological processes could help convert arctic  
9 tundra to shrubland, *Bioscience*, 55, 17-26, 2005.

10 Sullivan, P. F.: Snow distribution, soil temperature and late winter CO<sub>2</sub> efflux from soils near  
11 the Arctic treeline in northwest Alaska, *Biogeochemistry*, 99, 65-77, 2010.

12 Tabatabaenejad, A., Burgin, M., Duan, X. Y., and Moghaddam, M.: P-Band Radar Retrieval of  
13 Subsurface Soil Moisture Profile as a Second-Order Polynomial: First AirMOSS Results, *IEEE*  
14 *T Geosci Remote*, 53, 645-658, 2015.

15 Tape, K., Sturm, M., and Racine, C.: The evidence for shrub expansion in Northern Alaska and  
16 the Pan-Arctic, *Global Change Biology*, 12, 686-702, 2006.

17 Thornton, P. E., Law, B. E., Gholz, H. L., Clark, K. L., Falge, E., Ellsworth, D. S., Golstein, A.  
18 H., Monson, R. K., Hollinger, D., Falk, M., Chen, J., and Sparks, J. P.: Modeling and measuring  
19 the effects of disturbance history and climate on carbon and water budgets in evergreen  
20 needleleaf forests, *Agricultural and Forest Meteorology*, 113, 185-222, 2002.

21 Waldrop, M. P., Wickland, K. P., White III, R., Berhe, A. A., Harden, J. W. and Romanovsky, V.  
22 E.: Molecular investigations into a globally important carbon pool: permafrost-protected carbon  
23 in Alaskan soils. *Global Change Biology*, 16: 2543-2554. doi: 10.1111/j.1365-  
24 2486.2009.02141.x. 2010.

25 Walker, D. A., Raynolds, M. K., Daniels, F. J. A., Einarsson, E., Elvebakk, A., Gould, W. A.,  
26 Katenin, A. E., Kholod, S. S., Markon, C. J., Melnikov, E. S., Moskalenko, N. G., Talbot, S. S.,  
27 Yurtsev, B. A., and Team, C.: The Circumpolar Arctic vegetation map, *J Veg Sci*, 16, 267-282,  
28 2005.



- 1 Watts, J. D., Kimball, J. S., Jones, L. A., Schroeder, R., and McDonald, K. C.: Satellite  
2 Microwave remote sensing of contrasting surface water inundation changes within the Arctic–  
3 Boreal Region, *Remote Sens Environ*, 127, 223-236, 2012.
- 4 Weedon, G. P., Balsamo, G., Bellouin, N., Gomes, S., Best, M. J., and Viterbo, P.: The WFDEI  
5 meteorological forcing data set: WATCH Forcing Data methodology applied to ERA-Interim  
6 reanalysis data, *Water Resources Research*, 50, 7505-7514, 2014.
- 7 White, M. A., Thornton, P. E., Running, S. W., and Nemani, R. R.: Parameterization and  
8 Sensitivity Analysis of the BIOME–BGC Terrestrial Ecosystem Model: Net Primary Production  
9 Controls, *Earth Interactions*, 4, 1-85, 2000.
- 10 Xu, L., Myneni, R. B., Chapin III, F. S., Callaghan, T. V., Pinzon, J. E., Tucker, C. J., Zhu, Z., Bi,  
11 J., Ciais, P., Tømmervik, H., Euskirchen, E. S., Forbes, B. C., Piao, S. L., Anderson, B. T.,  
12 Ganguly, S., Nemani, R. R., Goetz, S. J., Beck, P. S. A., Bunn, A. G., Cao, C., and Stroeve, J. C.:  
13 Temperature and vegetation seasonality diminishment over northern lands, *Nature Climate  
14 Change*, 3, 581-586, doi:10.1038/nclimate1836, 2013.
- 15 Yi, Y., Kimball, J. S., Jones, L. A., Reichle, R. H., Nemani, R., and Margolis, H. A.: Recent  
16 climate and fire disturbance impacts on boreal and arctic ecosystem productivity estimated using  
17 a satellite-based terrestrial carbon flux model, *J Geophys Res-Biogeophys*, 118, 606-622, 2013.
- 18 Yi, Y., Kimball, J. S., and Reichle, R. H.: Spring hydrology determines summer net carbon  
19 uptake in northern ecosystems, *Environ. Res. Lett.*, 9, 064003, doi:10.1088/1748-  
20 9326/9/6/064003, 2014.
- 21 Zhang, T.: Influence of the seasonal snow cover on the ground thermal regime: an overview,  
22 *Rev. Geophys.*, 43, RG4002, doi:10.1029/2004RG000157, 2005.
- 23 Zhang, T., Frauenfeld, O. W., Serreze, M. C., Etringer, A., Oelke, C., McCreight, J., Barry, R. G.,  
24 Gilichinsky, D., Yang, D. Q., Ye, H. C., Ling, F., and Chudinova, S.: Spatial and temporal  
25 variability in active layer thickness over the Russian Arctic drainage basin, *J. Geophys. Res.-  
26 Atmos.*, 110, D16101, doi:10.1029/2004JD005642, 2005.

- 1 Zhang T., Heginbottom J A, Barry R G and Brown J: Further statistics on the distribution of
- 2 permafrost and ground ice in the northern hemisphere, *Polar Geography*, 24, 126-131, 2000.
- 3 Zimov, S. A., Davidov, S. P., Voropaev, Y. V., Prosiannikov, S. F., Semiletov, I. P., Chapin, M.
- 4 C., and Chapin, F. S.: Siberian CO<sub>2</sub> efflux in winter as a CO<sub>2</sub> source and cause of seasonality in
- 5 atmospheric CO<sub>2</sub>, *Climatic Change*, 33, 111-120, 1996.

1 Table 1. Characteristics of two selected tundra and boreal forest tower sites used for model  
 2 validation. Three tundra types are represented by the tower measurements at Imnavait Creek,  
 3 Alaska, including dry heath, moist acidic tussock and wet sedge tundra. The boreal forest site  
 4 encompasses a set of tower Eddy Covariance (EC) sites and measurements spanning a regional  
 5 fire chronosequence at various succession stages in central Manitoba, Canada.

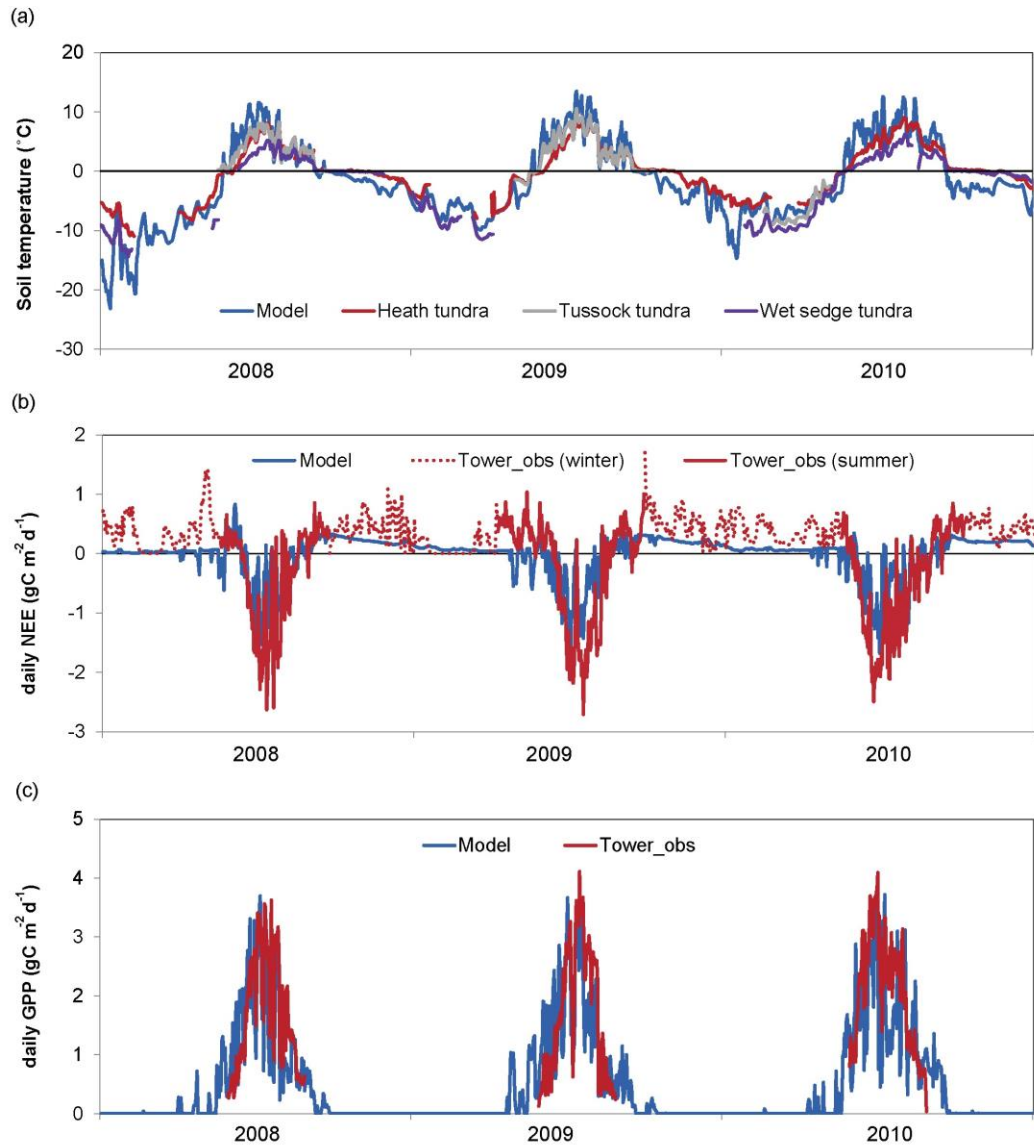
	Tundra	Boreal forest
Site	Imnavait Creek, AK	Manitoba, Canada
Location (Lat, Lon)	68°37'N, 149°18'W	55°54'N, 98°31'W
Permafrost	Continuous permafrost	No
Observation period	2008-2011	2002-2005
Soil temperature measurement depths (cm)	0, 5	0, 6,11,16,18,29,41,55
Soil moisture measurements depths (cm)	5	11,18,28,41,55

6

1 Table 2. Coefficient of determination ( $R^2$ ) and root mean square error (RMSE) differences  
 2 between model simulated daily carbon fluxes and in situ tower EC measurement based  
 3 observations across the study area. The mean of tower-observed daily GPP flux is also shown.  
 4 The uncertainty of the estimates including mean,  $R^2$  and RMSE values was indicated as a  
 5 standard deviation when there were multiple sites represented for each plant functional type.

PFT	Tower sites	GPP			NEE	
		Mean ( $\text{gC m}^{-2} \text{d}^{-1}$ )	$R^2$	RMSE ( $\text{gC m}^{-2} \text{d}^{-1}$ )	$R^2$	RMSE ( $\text{gC m}^{-2} \text{d}^{-1}$ )
ENF	12	2.18±1.23	0.70±0.17	1.46±0.59	0.34±0.15	1.06±0.40
DBF	2	2.11±0.96	0.82±0.02	1.31±0.60	0.59±0.04	1.29±0.39
MXF	3	1.99±1.02	0.77±0.03	1.46±0.45	0.58±0.11	1.00±0.29
GRS	1	1.87	0.92	1.38	0.89	1.12
WET	1	0.77	0.83	1.23	0.71	0.75
Tundra	1	0.39	0.62	1.76	0.38	0.66

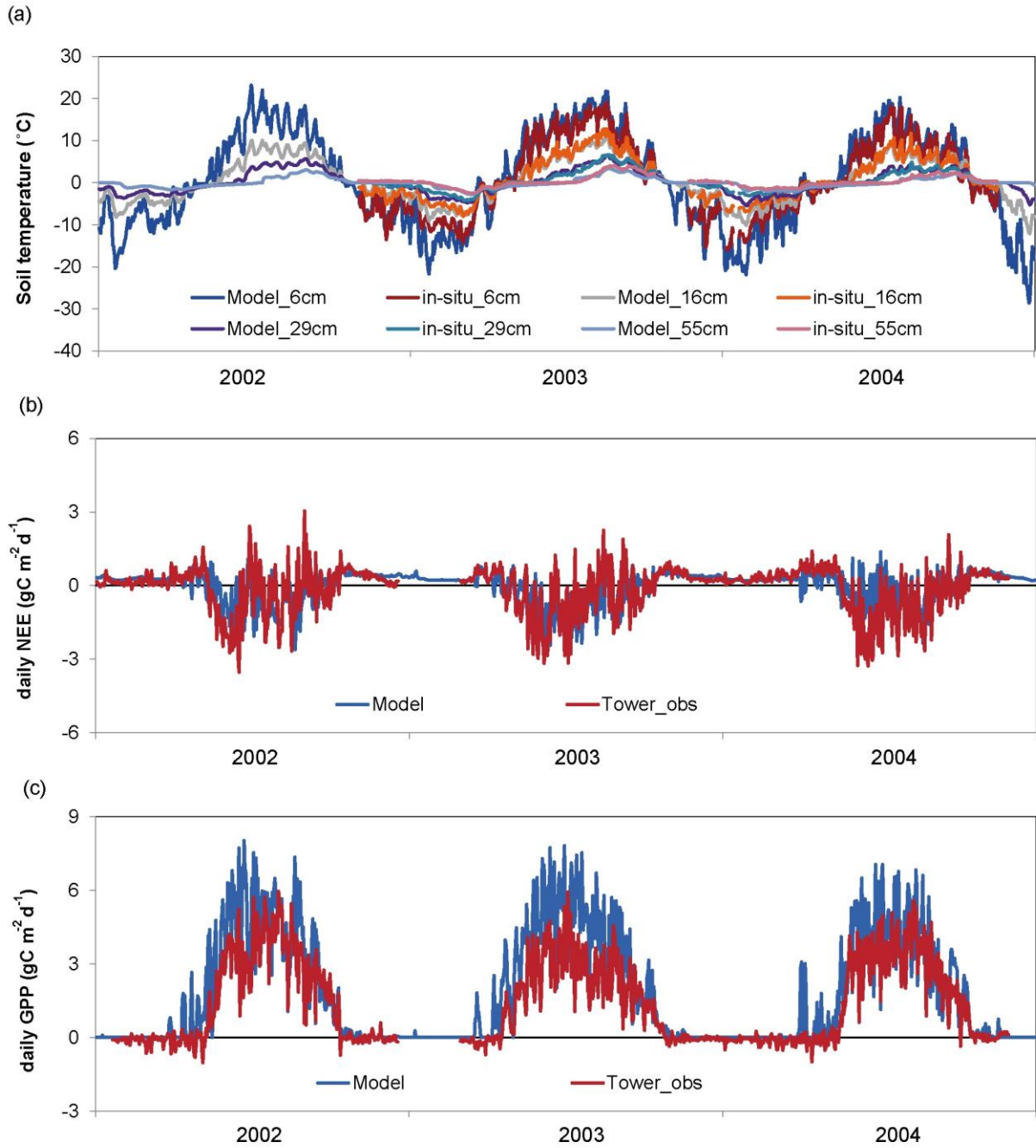
6 PFT (plant functional type): evergreen needle-leaf forest; DBF: deciduous broadleaf forest; MXF:  
 7 mixed forest; GRS: grassland; WET: wetland.



1  
2

3 Figure 1. Comparisons of model simulated (a) surface soil temperature (~5 cm depth) and carbon  
 4 fluxes (b: NEE and c: GPP), and tower measurements at the Innavait Creek, Alaska tundra sites,  
 5 over a three year (2008-2010) daily record. The tower observed carbon fluxes were averaged  
 6 across three tundra community types, including dry heath, moist acidic tussock and wet sedge  
 7 tundra except for the NEE measurements during the winter. NEE measurements were not  
 8 collected at the tussock tundra site during the winter; therefore, the winter NEE measurements  
 9 were averaged for the dry heath and wet sedge tundra sites only.

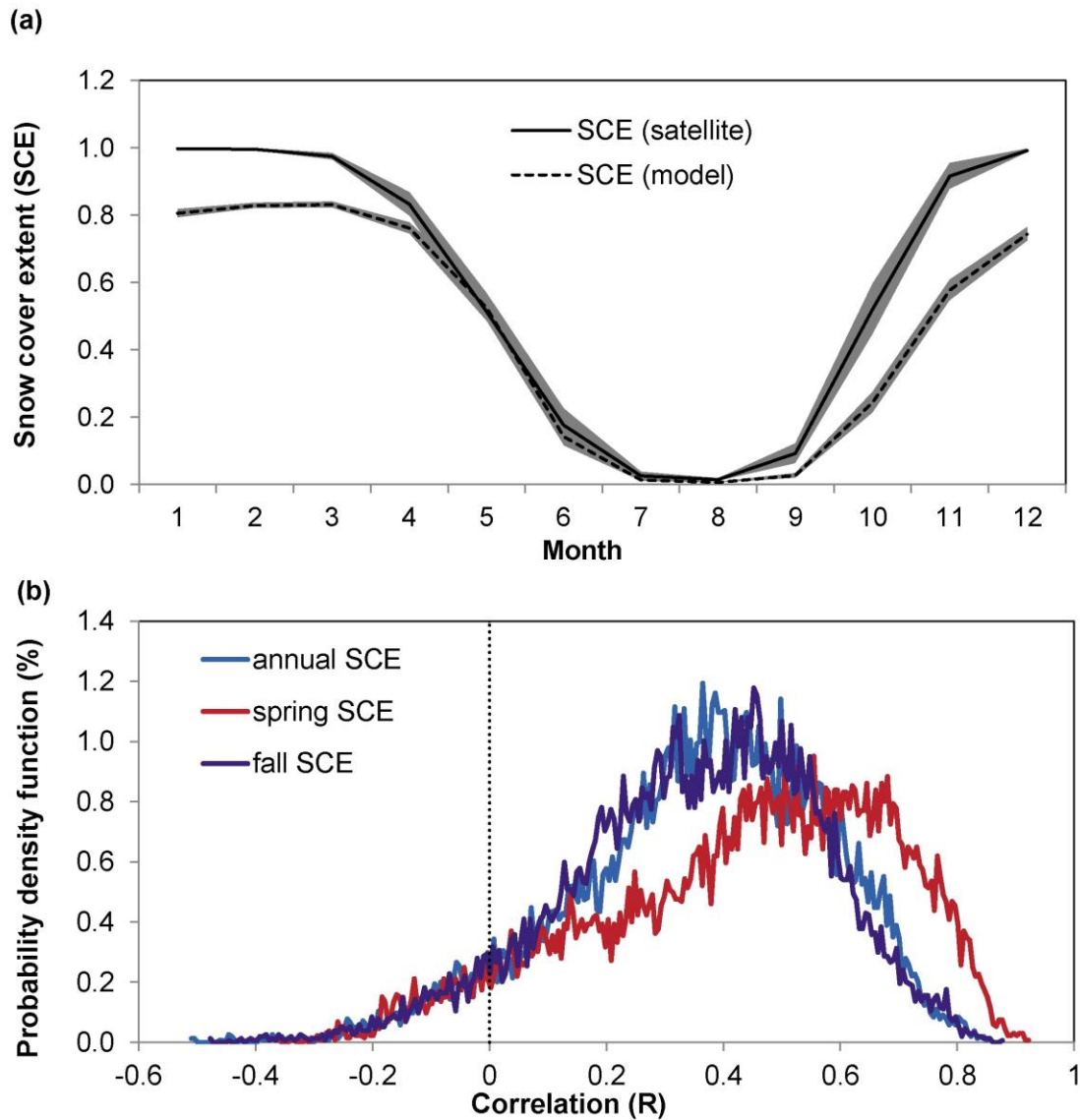
10



1  
2  
3  
4  
5  
6

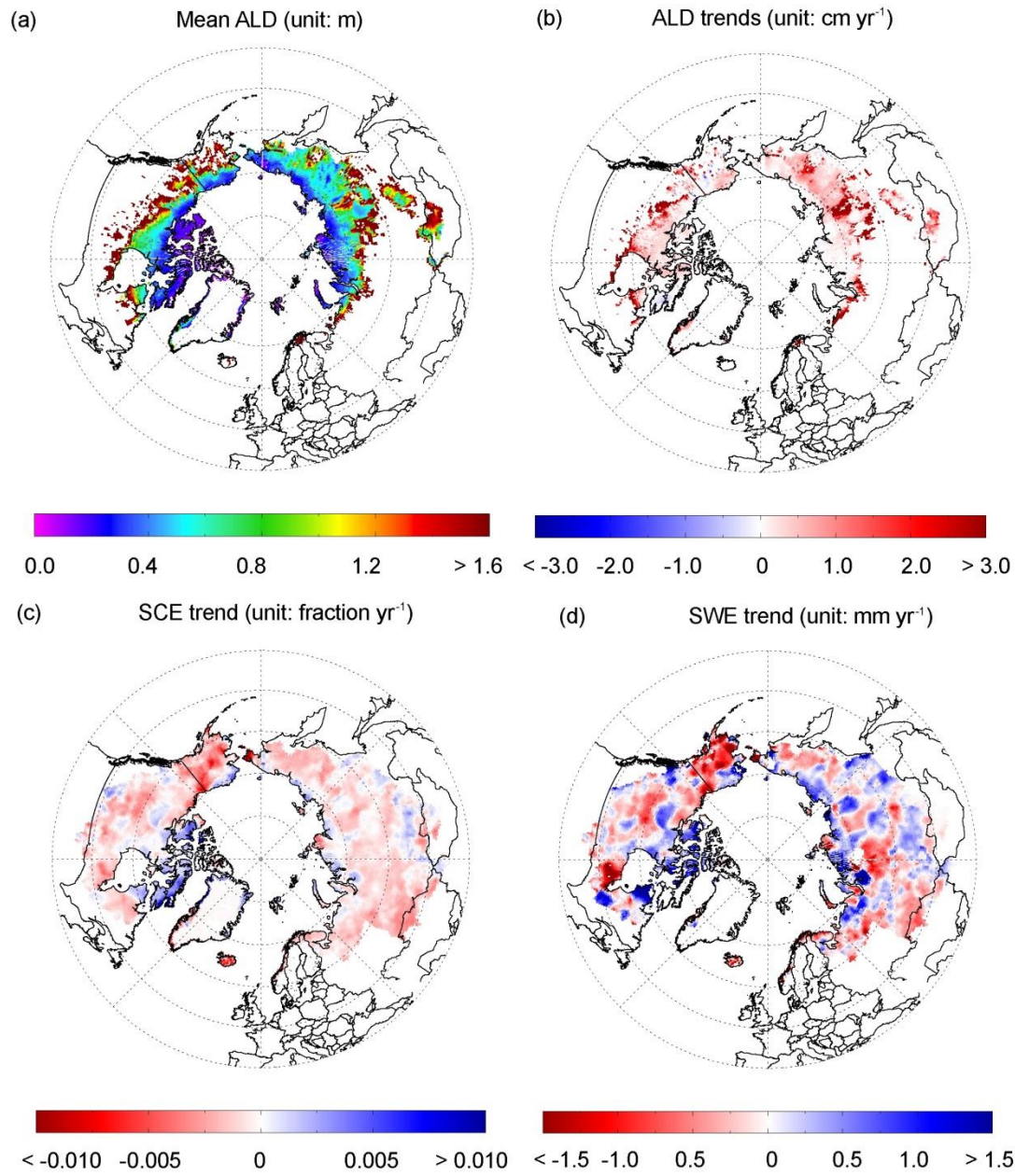
Figure 2. Comparisons of model simulated (a) soil temperature at different depths (6, 16, 29, and 55 cm) and carbon fluxes (b: NEE and c: GPP), and tower measurements at a mature boreal forest site in Manitoba, Canada over a three year (2002-2004) daily record.

1



2

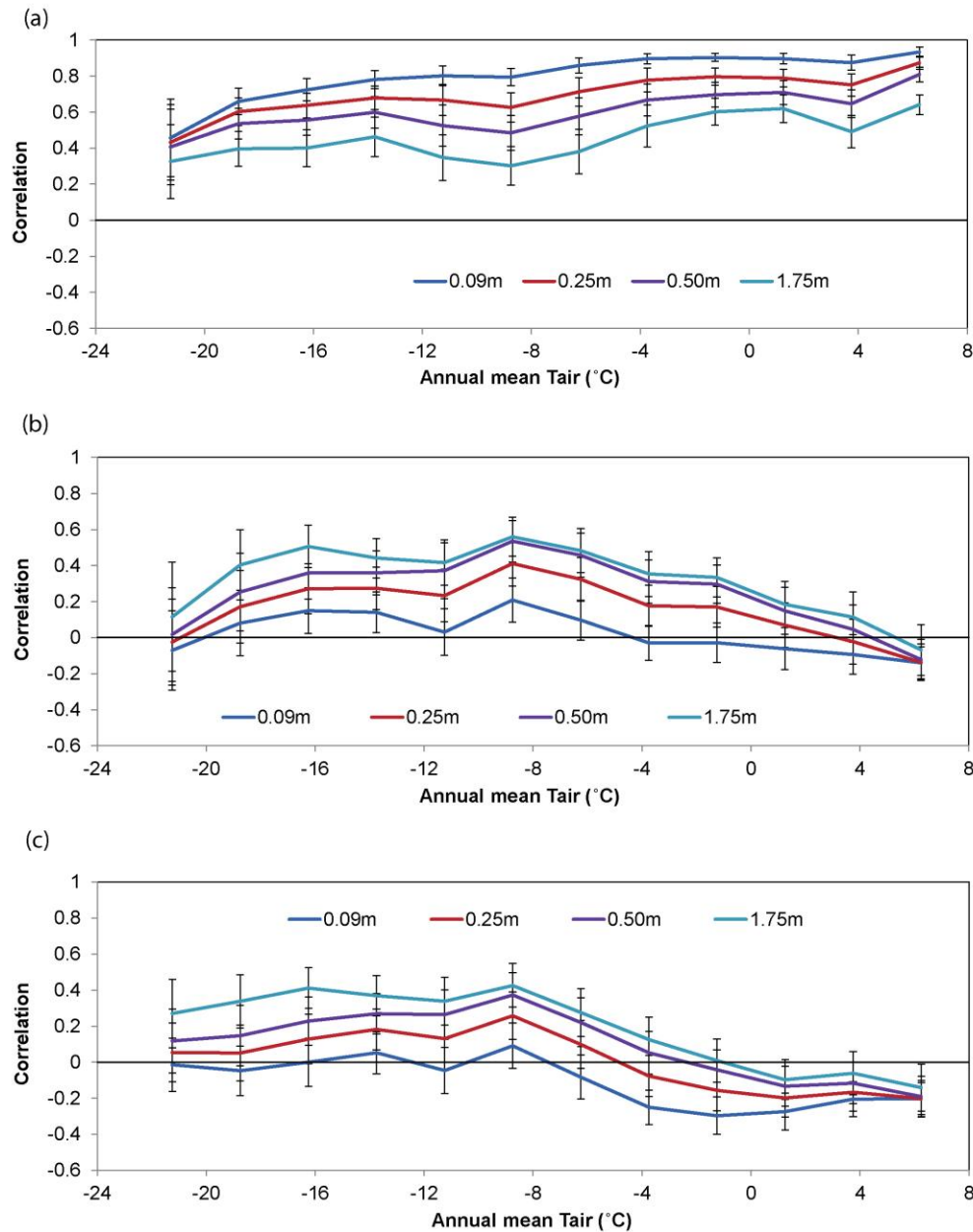
3 Fig. 3 Comparisons of model simulations and satellite-based climate data records (CDR) of snow  
4 cover extent (SCE; Brown and Robinson 2011) over the pan-Arctic modeling domain. (a) The  
5 seasonal cycle of modeled and satellite observed SCE; (b) the probability density function of the  
6 correlation coefficient (R) between modeled and satellite observed SCE at annual and seasonal  
7 time scales (spring: March to May; fall: September to November) from 1982 to 2010. Gray  
8 shading (a) denotes the temporal standard deviation from the multi-year means for the 1982 to  
9 2010 record.



1  
2  
3  
4  
5  
6  
7  
8

Figure 4. Model simulated spatial pattern of active layer depth (ALD, a) and estimated trends in ALD (b), snow cover extent (SCE, c) and snow water equivalent (SWE, d) over the pan-Arctic basin and Alaska domain from 1982 to 2010. Areas in white are non-permafrost areas (a, b) or outside of the modeling domain.

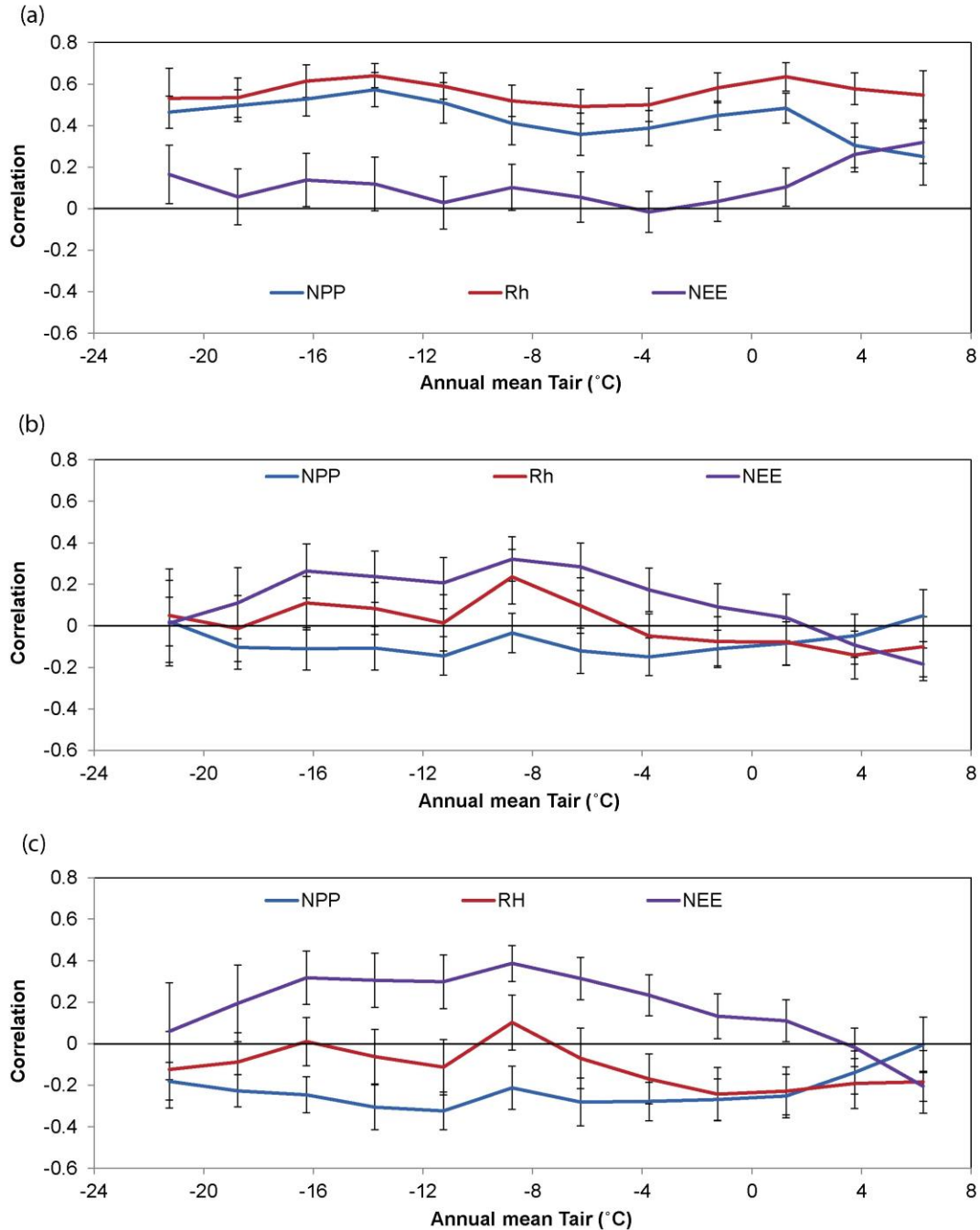




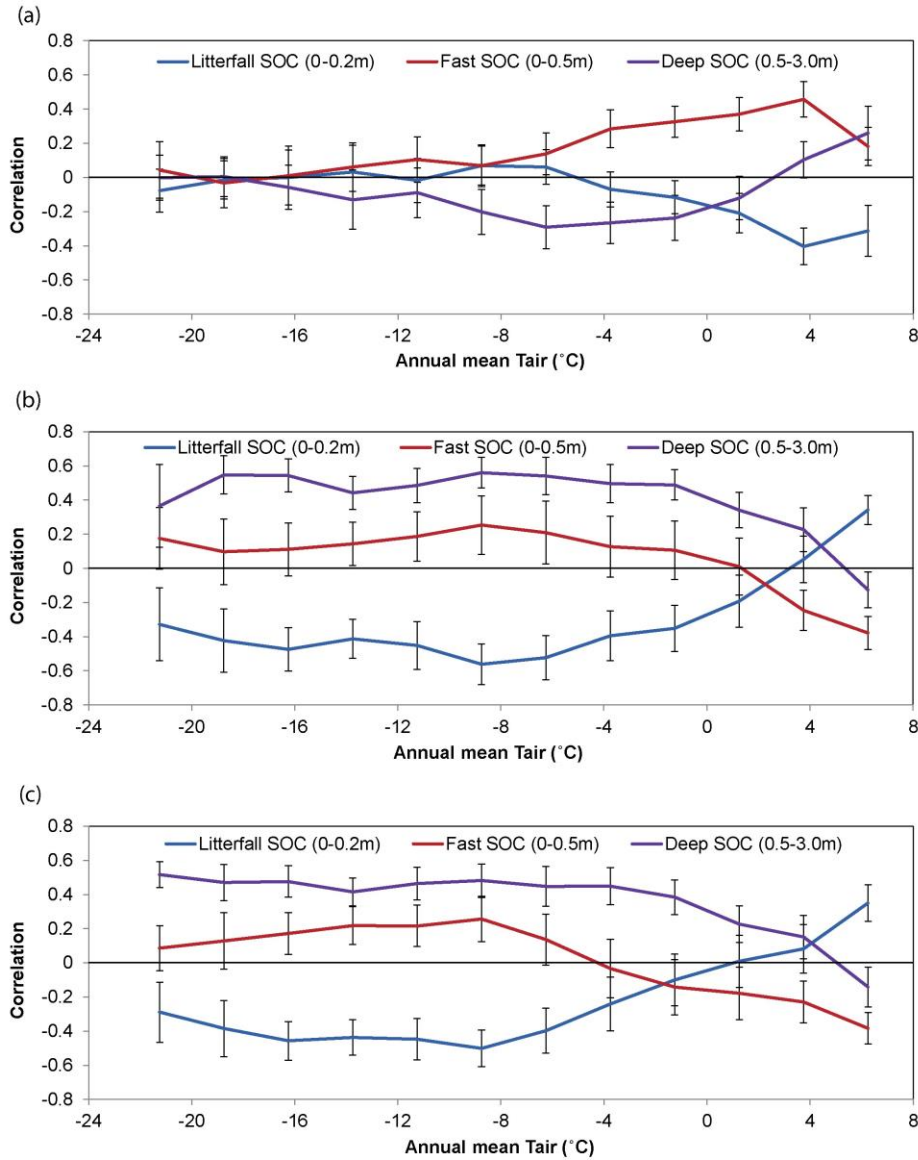
1

2

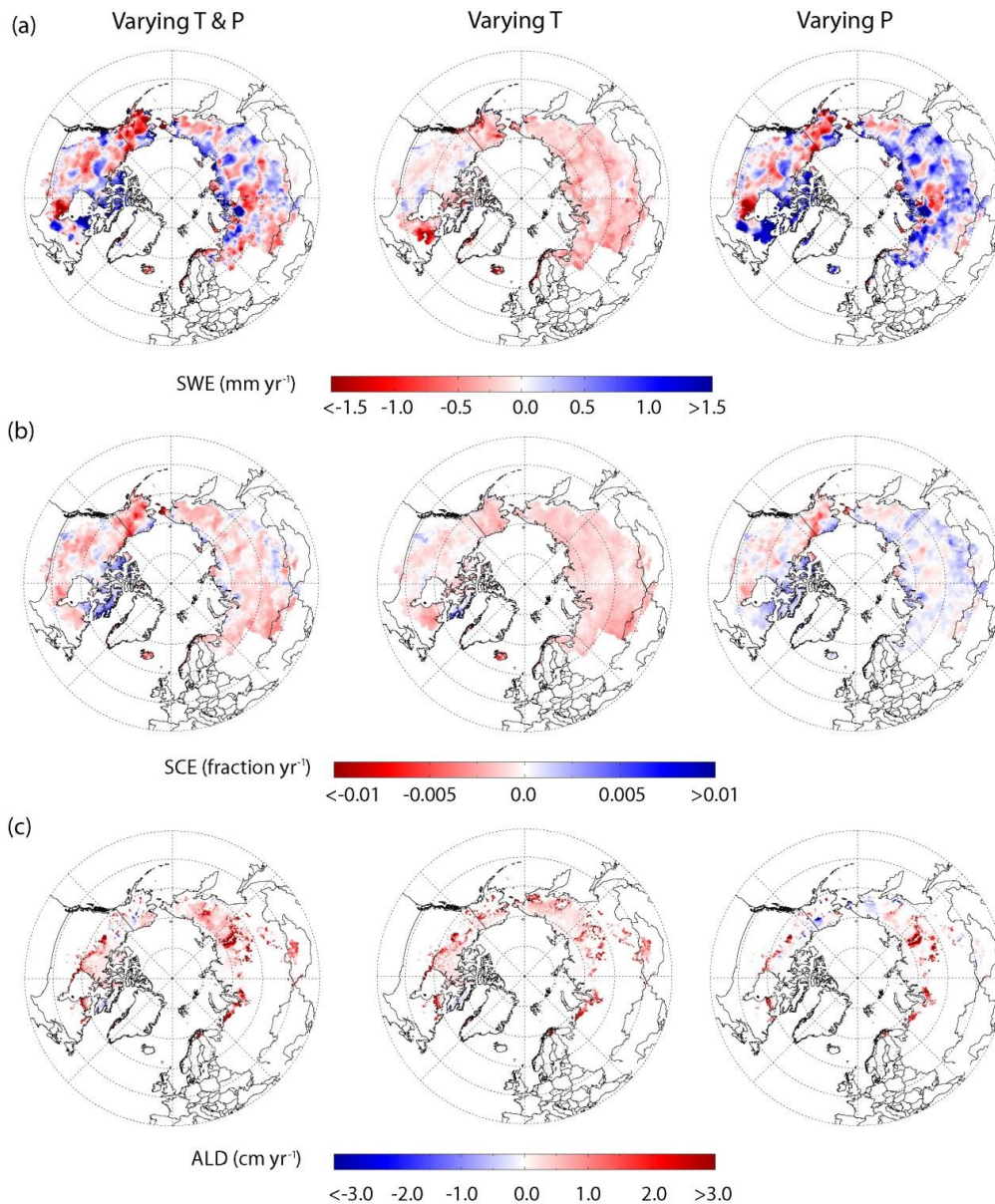
3 Figure 5. Correlations between climate variables and warm-season (May-October) soil  
 4 temperature at different soil depths (0.09, 0.25, 0.50 and 1.75 m). The climate variables used for  
 5 correlation analysis in each panel are: (a) warm-season air temperature (Tair), (b) pre-season  
 6 snow water equivalent (SWE) and (c) pre-season snow cover extent (SCE). The pre-season is  
 7 defined from November of the previous year to April of this year. The correlations were binned  
 8 into 2.5 °C intervals. The standard deviation of correlations across each climate zone is shown by  
 9 the error bars.



1  
 2 Figure 6. Correlations between annual carbon fluxes and climate variables including (a) annual  
 3 mean air temperature, (b) annual mean snow water equivalent (SWE), and (c) annual mean snow  
 4 cover extent (SCE). The annual carbon fluxes include NEE and its two component fluxes (i.e.  
 5 NPP and soil heterotrophic respiration Rh). The correlations were binned into 2.5 °C intervals.  
 6 The standard deviation of correlations across each climate zone is shown by the error bars.



1  
 2 Figure 7. Correlations between climate variables and warm-season (May-October) soil  
 3 heterotrophic respiration (Rh) contribution from different soil organic carbon (SOC) pools (i.e.  
 4 Rh fraction). The climate variables used for the correlation analysis in each panel are: (a) warm-  
 5 season air temperature (Tair), (b) preseason snow water equivalent (SWE), and (c) preseason  
 6 snow cover extent (SCE). The correlations were binned into 2.5 °C intervals. The 3 litterfall  
 7 SOC pools were distributed at the top 0.2 m of the soil layers; the 3 SOC pools with fast turnover  
 8 rates were distributed in the top 0.5 m of the soil layers; the deep SOC pool with slow turnover  
 9 rates extended from 0.5 m to 3 m below surface. The standard deviation of correlations across  
 10 each climate zone is shown by the error bars.

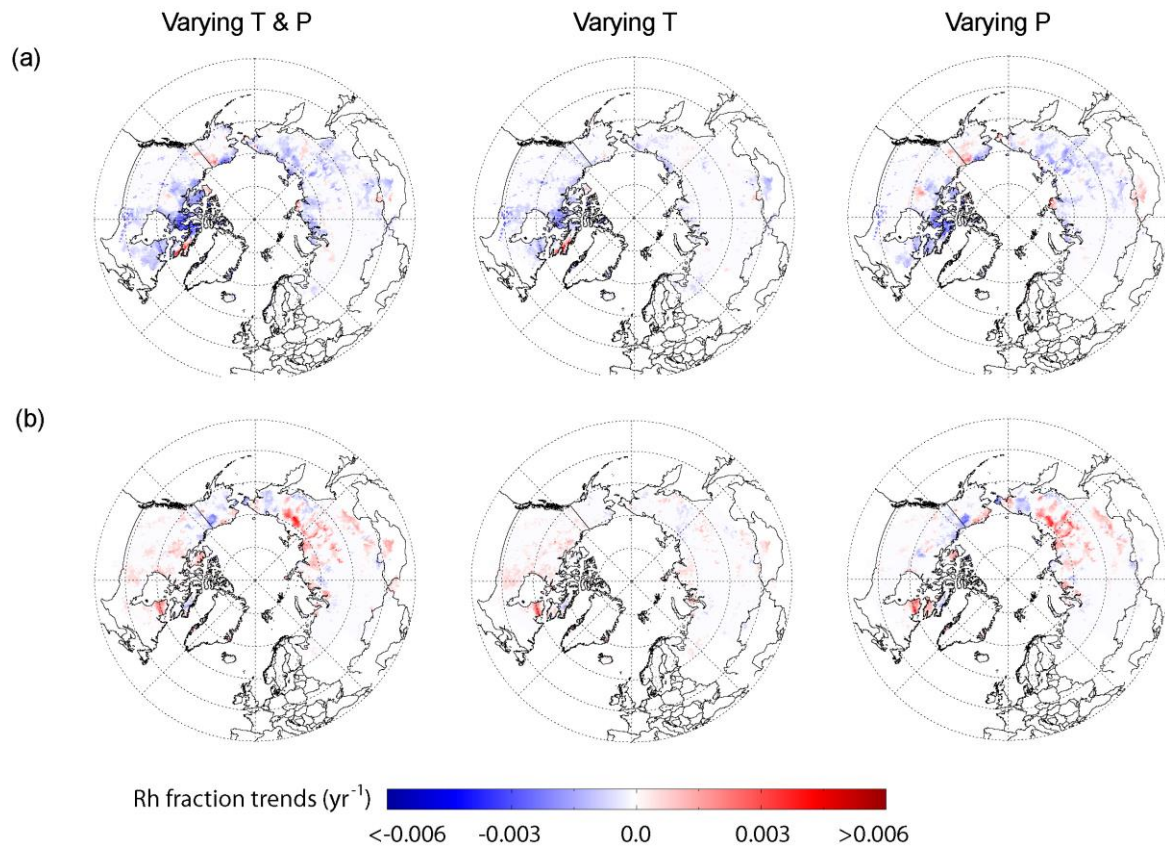


1

2

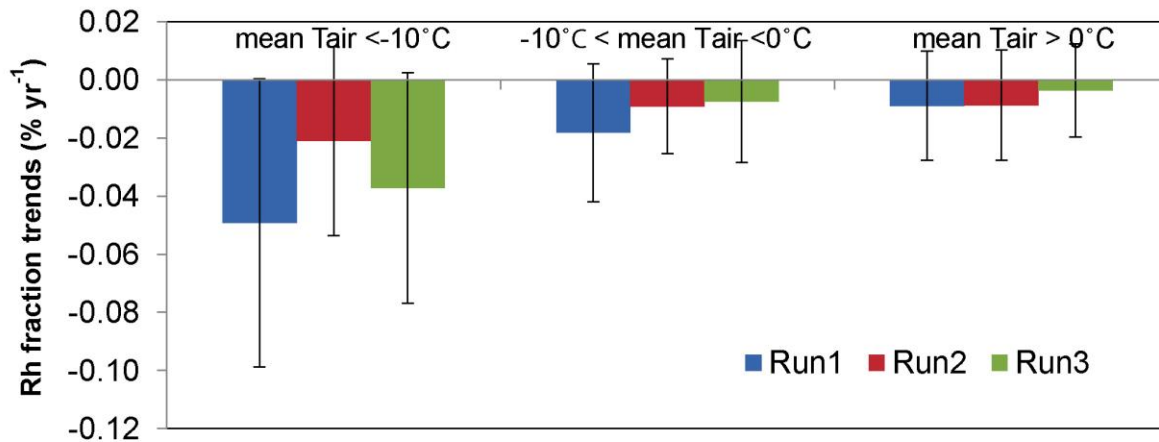
3 Figure 8. Simulated trends of (a) snow water equivalent (SWE), (b) snow cover extent (SCE) and  
 4 (c) active layer depth (ALD) for the three model sensitivity experiments for the 1982 to 2010  
 5 period. For the sensitivity analysis, the model was driven using different surface meteorology  
 6 datasets. The results based on model runs using varying temperature (T) and precipitation (P) are  
 7 presented in the left column; the results based on model runs using varying T alone are shown in  
 8 the middle column, and results based on model runs using varying P alone are shown in the right  
 9 column.

10

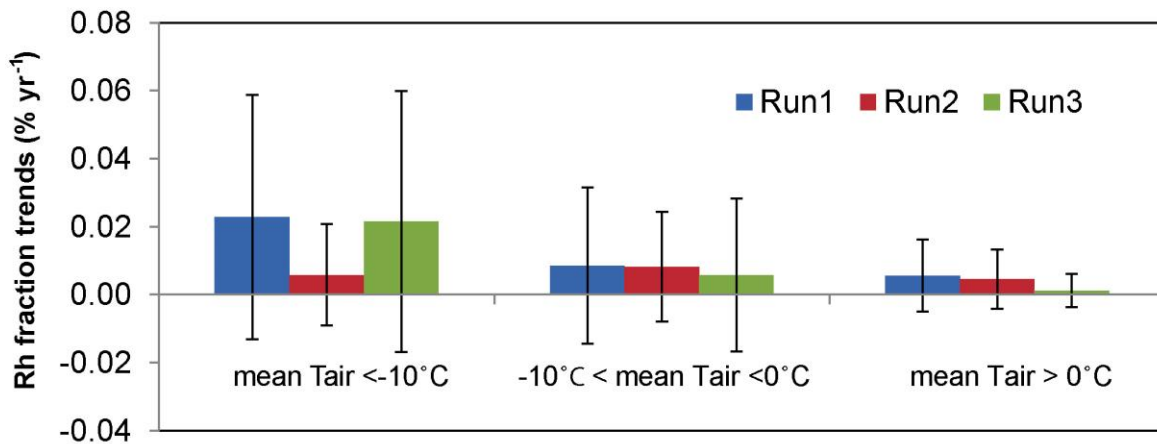


1  
 2 Figure 9. Similar to Fig. 8, but for simulated trends (unit:  $\text{yr}^{-1}$ ) of the warm-season (May-October)  
 3 soil heterotrophic respiration (Rh) contribution (i.e. Rh fraction) from (a) surface (0-0.2 m) and  
 4 (b) deep (0.5-3.0 m) soil carbon pools for the three sensitivity experiments using different  
 5 surface meteorology configurations, i.e. varying temperature (T) and precipitation (P) inputs,  
 6 from 1982 to 2010.

(a)



(b)



1

2

3 Figure 10. The zonal-average trends of warm-season (May-October) soil heterotrophic  
4 respiration (Rh) contribution (i.e. Rh fraction) from (a) surface litterfall (0-0.2 m) and (b) deep  
5 (0.5-3.0 m) soil carbon pools for the three sensitivity experiments from 1982 to 2010. Run1  
6 indicates model simulations based on varying temperature (T) and precipitation (P) inputs; Run2  
7 indicates model simulations based on varying T inputs alone; and Run3 indicates model  
8 simulations based on varying P inputs alone.